MASTER THESIS

Characterization of Reactive Oxygen Species Responsive Copolymeric Micelles for Drug Delivery Purposes

By

Pepijn R. Bouwmans

In partial fulfillment of the requirements for the degree of Master of Science in Chemical Engineering

at Delft University of Technology,

To be defended on February 18, 2021

Student number:	4274156
Educational Program:	MSc Chemical Engineering
Project duration:	March 12, 2020 - February 18, 2021
Institution:	Delft University of Technology
Faculty:	Applied Sciences
Departments | Research Groups:	Radiation Science & Technology | Applied Radiation & Isotopes (ARI) (Reactor Institute Delft)
	Chemical Engineering | Advanced Soft Matter (ASM)
Supervisors:	Dr.ir. Antonia Denkova & Dr. Rienk Eelkema
Daily supervisors:	Irene Piergentilli, MSc & Dr. Reece Lewis
Thesis Committee:	Dr.ir Antonia Denkova
	Dr. Rienk Eelkema
	Dr. Kristina Djanashvili

Acknowledgements

Firstly, I would like to thank my supervisors, Antonia and Rienk, for the opportunity to do a practical research and keeping me in track with valuable feedback during all the progress meetings. Secondly, I would like to thank Irene and Reece, for getting me familiar within the lab, teaching me to interpret data and motivating me throughout the project. Furthermore, I would like to thank Huanhuan, for helping me around the labs and for the valuable solutions of practical problems. And I would like to thank Kristina, for being member of the thesis committee. Lastly, I would like to thank both ARI and ASM for having me, I really enjoyed the time, especially in the labs.

Abstract

Treatment of cancer requires local medication at the tumor site to prevent side-effects of chemotherapy. Nanocarriers, such as micelles, can be used to transport drugs to the tumor site and limit side effects of cancer treatment. Micelles are easy to produce, have a high solubilization potential for hydrophobic drugs and therefore can have high loading capacity. Due to the increase in cell division and higher activity of cancer cells, elevated levels of reactive oxygen species (ROS) are often present at the tumor site. ROS have a highly oxidizing agent property by damaging DNA of cancer cells, it can be used to treat tumors. Beside ROS formation of the metabolic cycle, ROS can also be produced by ionizing radiation. With radiolysis of water, caused by radiation, the ROS concentrations at tumor sites can be increased. This research aimed to prepare micelles made from a block copolymer, that are sensitive to ROS and that are sensitive to ROS formed by radiolysis of water with gamma radiation for drug release purposes. 4-(methylthio)phenyl acrylate (MTPA) groups present in the block copolymer (PDMA-MTPA), are sensitive for oxidation reactions which will lead to decomposition of the polymer, and thus of the micelles. During this research, micelles with a hydrodynamic diameter between 30 and 50 nm were exposed to H_2O_2 levels between 2 wt% (0.6 M) and 0.007 wt% (2 mM) and a change in hydrodynamic diameter and light intensity scattering was observed, meaning that micelles decompose with elevated concentrations of H_2O_2. In addition, an increase in hydrodynamic diameter was observed for micelles exposed to a dose between 67 and 500 Gray by irradiating with gamma rays of 1.25 MeV originating from a ^{60}Co source, indicating that micelles cluster after sufficient dose of gamma radiation. These characteristics can be useful for making PDMA-MTPA micelles, a suitable candidate for drug delivery applications.

Table of content

Abbreviations

- AFM: Atomic force microscopy
- Cps: counts per second
- Cryo-EM: Cryogenic electron microscopy
- DLS: Dynamic light scattering
- DMA: N,N- dimethylacrylamide
- DOTA: 1,4,7,10-tetraazacyclododecane-1,4,7,10- tetraacetic acid
- DOX: Hydrophobic doxorubicin
- GPC: Gel permeation chromatography
- GSH: Glutathione
- Gy: Gray
- HEPES: 4-(2-hydroxyethyl)-1-piperazineethanesulfonic acid buffer (100 mM 7.4 pH)
- ^{1}H-NMR: Proton nuclear magnetic resonance
- kDa: kiloDalton
- Kcps: kilo counts per second
- MTPA: 4-(methylthio)phenyl acrylate
- NR: Nile Red
- PB: Phosphate based buffer (100mM, 7.4pH)
- PDI: polydispersity index
- PDMA-MTPA: block copolymer made from DMA and MTPA
- $PD_{85}M_{26}$: Block copolymer with 85 DMA and 26 MTPA groups
- $PD_{130}M_{16}$: Block copolymer with 130 DMA and 16 MTPA groups
- $PD_XM_{Y:}$ Generic term that both $PD_{85}M_{26}$ and $PD_{130}M_{16}$ are used separately for the same experiment
- PET: Positron emission tomography
- PSMA: Prostate-specific membrane antigen
- RI: Refractive index
- ROS: Reactive oxygen species
- SOD: Superoxide dismutase
- SOPh: 4-(methylsulfinyl)phenol
- SO_2Ph: 4-(methylsulfonyl)phenol
- SPh: 4-(methylthio)phenol
- t: Time
- T: Temperature
- TEM: Transmission electron microscopy

Introduction

Cancer is a common cause of death in the world. More than 1,500,000 U.S. citizens are diagnosed with cancer each year and over 500,000 U.S. citizens will die due to cancer.[1] Patients diagnosed with cancer can undergo different forms of treatments. Often used treatment strategies consist of combinations of surgery, chemotherapy and radiation.[2] After chemotherapy, most people are affected with many side effects, which can occur when medication is not tumor specific. This can result in damaging many other organs and tissues, beside the tumor. In order to protect healthy tissue from aggressive medication, drug delivery systems could be used as alternative treatment strategy.[3]

Drug delivery systems

Drug delivery systems are carriers or nanoparticles, including liposomes, polymerosomes and micelles, but also gold particles and nanocrystals, which can encapsulate a medicine or have a medical property. Drug delivery systems can function by accumulating at the tumor site and releasing the drug in response to a certain signal within or around the tumor cell. Tumor sites have different characteristics compared to healthy tissue including a difference in pH[4], increase in blood flow[5], overexpression of receptors on tumor cells [6] and higher metabolic activity.[7] These tumor specific properties can be used as a signal in order to trigger drug delivery systems to release their drug. The higher metabolic activity of these cells corresponds to an increase in energy requirement, resulting in the production of more reactive oxygen species (ROS). These characteristics lead to an increased interest towards the investigation and design of nanocarriers responsive to ROS, such as micelles which are loaded with doxorubicin (DOX), for drug release purposes. [4,8,9,10,11,12] Micelles can function as a drug delivery system and require an increased blood flow to accumulate at the tumor site where an increase in ROS is a key signal for drug release. Micelles have the advantage that they are easily formed, are water soluble, have selective targeting (compared to conventional chemotherapy drugs), limit side effects and can contain a high drug loading.[13]

Reactive oxygen species

Molecular oxygen is in its stable form a biradical and has two half-filled orbitals, this is one of the reasons why oxygen is a good electron acceptor. [14] In many biological processes oxygen is converted to water after accepting the electrons and protons, such as the metabolic cycle.[15] After accepting an electron, oxygen can be converted sometimes (1 up to 2 %) into a different oxygen species such as superoxide.[16] Superoxide can be converted into hydrogen peroxide (H_2O_2) by superoxide dismutase (SOD), the H_2O_2 is converted to water and oxygen by catalase. ROS are oxygen-based molecules, being a strong oxidizing agent, leading to high reactivity.

When ROS are not restrained in vivo, ROS can react with DNA and break bonds, this process is called oxidative stress. To protect cells and DNA from oxidative stress, antioxidants interfere with ROS. Many types of enzymes assist to keep ROS concentrations low in cells at different organelles, such as the earlier mentioned SOD and catalase.[15] Besides enzymes, different organic compounds also assist in limiting ROS concentrations, such as vitamins including vitamins A, C and E.

In contrast to the in vivo production of ROS, ROS can also be produced experimentally. One method to produce ROS, is with catalyst the TiO, TiO behaves as an electron donor or electron acceptor (holes).[17] Another method to generate ROS is by usage of ionizing radiation, such as alpha beta or gamma radiation in water. Ionizing radiation, can collide with electrons and by ejecting these electrons, ROS are produced. The amount of ROS formed is dependent on the dose expressed in gray the medium receives. A final example is the “trojan horse”, a recent drug delivery system. This promising drug carrier elevates the levels of ROS by addition of certain amino acids, which causes the cell to overproduce ROS.[18,19] In order to detect ROS, specific or non-specific probes can be added which can react with ROS. These probes can be measured for example by a change in emission after oxidation by ROS.[20,21,22] However, due to the high reactiveness of radical based ROS, the chance exist that ROS reacts first with its environment instead of with a probe. Therefore, in vivo detection of ROS is both difficult and can be inaccurate.

ROS production in vivo

Cell signaling uses a mechanical or biochemical signal to communicate between different cells. ROS can be used for in vivo cell signalling[23,24,25] But beside signaling, it is believed that oxidative stress caused by ROS is the main reason that people age[26], is partly the cause of Alzheimer disease[27] and ROS are overexpressed in cancer. There are over 100 different forms of cancer and all these forms have in common that mutations in genes cause excessive duplication of malfunctioning cells.[28] These malfunctioning cells compete with healthy cells and can cause in a further stage deformations of body parts or organs. These mutations can be caused in several ways. Many types of cancer have a strong correlation with genetic deviations. Some people have certain genes which correlate to a higher chance of developing certain forms of cancer. For example, the genetic code for breast cancer. Other mutations can be caused by environment. Bad eating habits, correlate to an increased amount of colon cancer and smoking correlates to an increase amount of cancer in the lungs and throat.[29] Nowadays, the biggest steps forward in the battle against cancer are the diagnostics. [30] Cases where cancer is detected in an early stage, results in early stage treatment. [31] When cancer is in an immature state, treatment has a higher success rate.

Chemotherapy and radiation therapy can let the metastases mitigate and sometimes even lead to complete regression.[32] These therapies affect, besides tumors, also healthy tissue and organs. The drugs in chemotherapy have a destructive nature which causes side effects, chemotherapy can even lead to cancer. To minimize side effects from drugs, two kinds of targeting can be used: passive targeted drug delivery and active targeted drug delivery. Passive targeting is based on the retention time of the drug delivery system in the human body, using the physical properties that tumors possess, such as EPR effect. An example of active targeting for prostate cancer, is the PSMA ligand. This ligand is very specific for the acceptors at the prostate tissue and corresponds to PSMA receptors overexpressed at the tumor cells. Therefore, the ligand will mainly bind to tumors. This method is often used for diagnostics where beta plus decay particles is attached to PSMA with a chelator such as DOTA enabling PET imaging. Human tissue consists of cells where many processes occur, when glucose is consumed H_2O and CO_2 are produced. During the glucose cycle, oxygen is used as an electron acceptor and can, as previously mentioned, become a ROS. Within cells, three groups of organelles and one group of enzymes are known for ROS production: the mitochondria, peroxisomes, endoplasmatic reticulum and NADPH oxidases (Fig 2.1). Mitochondria are responsible for up to 80 % of oxygen consumption and therefore mitochondria are the main source of in vivo ROS productin.[33] Peroxisomes break down fatty acids and reduce the amount of radicals by forming H_2O_2. NADPH oxidase is an enzyme attached at the membrane of the cell which is used by the immune system or for signaling by using ROS. The endoplasmatic reticulum has a role in protein formation and protein transport, during the production ROS can be formed.

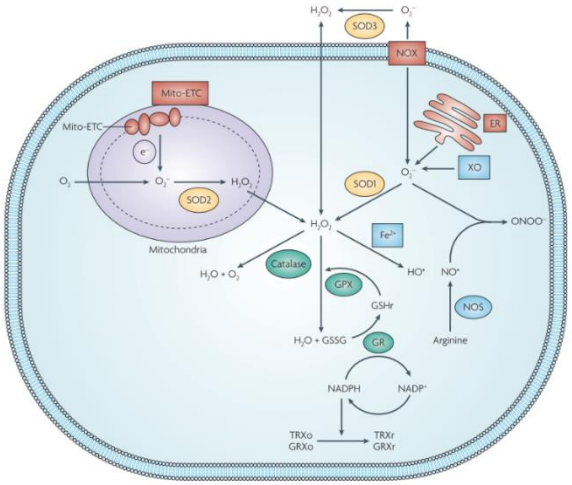

Fig (2.1) Schematic cell with main ROS productions pathways and main ROS interactions with antioxidants. This image was obtained from. [34]

Cancer grows faster compared to normal tissue, therefore all previous processes, which produce ROS, are increased. However, besides elevated ROS production, cancer tissue tends to be more resistant against ROS. Cancer has elevated levels of ROS scavengers (antioxidants such as GSH), which cause them to be more resistant against ROS, compared to normal tissue (Fig 2.2). Literature describes that higher ROS levels lead to higher cell survival of cancer and can make them drug resistant. Therefore, a treatment technique should not be based on just increasing ROS levels, because it will be relative more harmful to healthy tissue as to cancer tissue. When ROS concentrations are investigated in vivo, tissue is extracted and fed with nutrients to. By observing consumption of reactants and by reacting of ROS with probes, concentrations of ROS are determined. This will give a value of in vitro studies, and thus not in vivo. Because the probes can have uncertainty, by the relative short lifetime of ROS. In addition, due to heterogenous tissue of tumors, an average ROS concentration level can be misleading. However concentrations are reported that healthy (normal) tissue contains ROS concentrations in orders of nano or µM, whereas cancer cells at some specific sites contain ROS concentrations up to mM.[35]

Cancer has elevated levels of ROS and has an increased vascularity; however, cancer is not that straightforward and requires a more in dept understanding before a suitable drug release system can be made. The vascular system is often lacking behind in growth, meaning many cancer cells will die to limited blood flow. Furthermore, cancer is heterogeneous, tumors environment is different every few cells, and production of ROS will thus also differ per section of tumor. Additionally, the stage of the life cycle of the cell such as, stem cell, progenitor, or a cell with clear task, influences the amount of ROS. Stem cells are the fundamental of all cells since stem cells can be converted to all cells. Mistakes are crucial in that stage for the cells, thus stem cells have even higher levels of antioxidants such that the ROS will not damage cell production.[36]

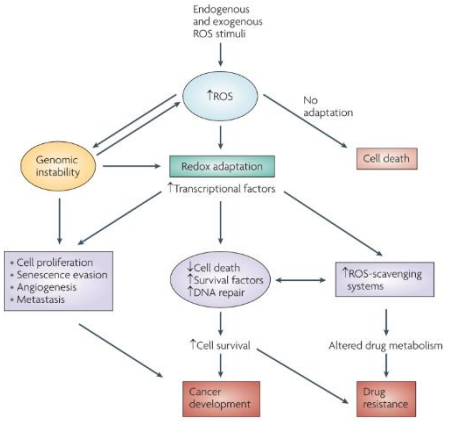

Fig (2.2) Cancer exposed to elevated levels of ROS. This image was obtained from. [34]

ROS production by ionizing radiation

During radiation therapy, depending on the type of cancer, alpha or beta radiation will be used for internal radiation. Gamma or x-rays will be used for external radiation. One way to produce gamma rays is by ^{60}Co decay. During the 1950's ^{60}Co therapy was used for irradiating cancer and over time mainly got replaced by x-rays produced by accelerators, which can create higher energetic particles, and no nuclear waste.[37] Applying external radiation by ^{60}Co decay, emits mainly gamma rays, one gamma around 1.17 MeV and one gamma around 1.33 MeV.[38,39] Gamma radiation in an aqueous solution, can form radicals by Compton effect. The number of radicals which will be formed correlates with two factors. First factor is the dose, which is expressed in gray (Gy), where one gray is equal to one joule/kg. Secondly, the type of radiation, for example, x-rays, gamma-, beta- or alpha radiation. The type of radiation is relevant due to cross-sections of interaction and if the radiation has sufficient energy to eject electrons and thus to form ROS. When ionizing radiation interacts with water forming ROS and these ROS interact with micelles, it is called an indirect effect. When the radiation directly interacts with micelles, this is called a direct effect. During radiation therapy, a dose of a few gray is used. This process can be repeated up to 30 times leading to a total radiation dose between 40 Gy and 100 Gy. From literature it is known that by external ^{60}Co radiation, a few Gy can only form few µM of H_2O_2. When increasing the total radiation dose up to 500 Gy, around 100 µM of H_2O_2 can be formed.[40]

Micelles (drug release) analytical techniques

To visualize morphological changes in drug delivery systems such as micelles, ^{1}H-NMR and Dynamic Light Scattering (DLS) is used. During this this thesis the Zetasizer was used, which for convenience is also called a DLS, specific specifications will thus not be applicable to all DLS devices. Furthermore, to identify the morphology of a certain nanoparticle, Transmission Electron Microscopy (TEM) and Cryogenic Electron Microscopy (Cryo-EM) are performed.

During this thesis, the hydrophobic part of micelles will be oxidized and hydrolyzed, this change within the polymer can be detected and visualized by ^{1}H-NMR. Beside ^{1}H-NMR for detection of decomposition, DLS can be used. DLS can show a change in distribution of particle size. When performing DLS, a laser at 633 nm shoots photons on the solution where the photon scatters from particles in solution. These photons are caught at 173.5-degree angle so only backscattering is observed. When particles are small around 10 times smaller than the wavelength of excitation light, they are called isotropic scattering centers.[41] With Rayleigh theory the amount of scattering in all directions is equal.[42] Thus if the detector is at 90 degrees or 173 degrees should provide the same result. However, using an angle of 173.5 degrees has three advantages. First, it excludes more random scattering between particles, making weak signal really correlate to a particle instead to random scattering. Secondly, it measures closer to the cuvette wall, making it able to measure more turbid systems. Lastly, the cuvette is about eight times more illuminated by orientation and thus more sensitive.[43,44] When particles become bigger than 100 nm in size, scattering will not be homogenous and measuring at different angles will give different results, which is explained by the Mie theory (Fig 2.3).[42]

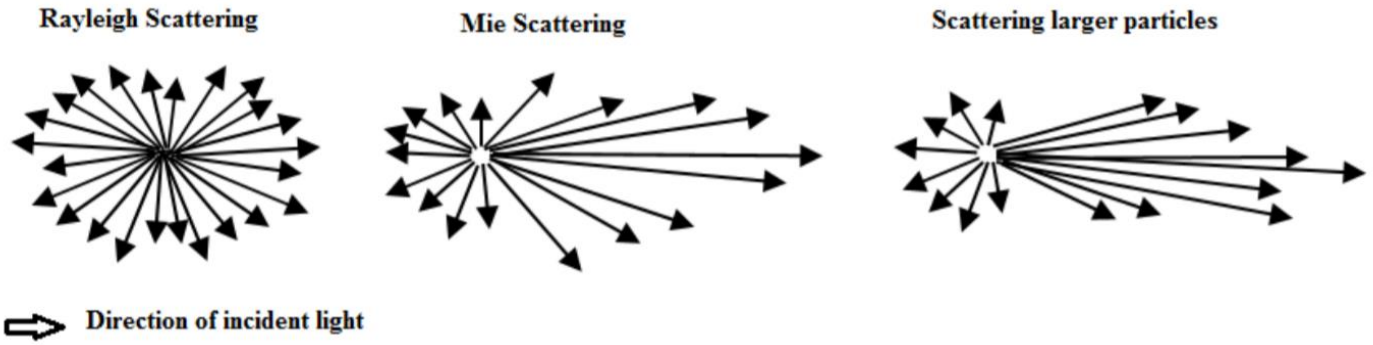

Fig 2.3 Rayleigh scattering Mie theory scattering and nonselective scattering. This image was obtained from.[45]

As long particles are below 100 nm size, measuring at solely 173 degree will be acceptable. In addition, the number of particles correlates to the amount of scattering. With too much light intensity scattering, often referred as scattering, the detector will be overloaded thus the laser will get an attenuator. An increase or decrease in attenuator will adjust light intensity by a factor of ~3. To process all data in one plot with different attenuators. The light intensity scattering data can be normalized, experience shows that the factor 3 is sometimes inaccurate, and can lead to extrapolated peaks. The detector forwards the signal to a correlogram, where the size and diffusion coefficient is determined. By using the Einstein-stokes equation, the size of a particle can be calculated with known diffusion coefficient and viscosity, and some assumptions.[39,43] For the Einstein stokes equation, the particle has to be a noncompressible spherical particle. Secondly, only one size can be considered so the particle needs to be monodisperse. For Brownian motion it is important that all particles have equal density. Lastly the optical parameters need to be known, including the refractive index of the solvent and the particles itself. Furthermore, for larger particles also scattering angles are important. It should be noted that particles in solution are never monodisperse which is necessary to calculate sizes exactly, meaning that sizes are always in size ranges.

However, when a polydispersity index (PDI) smaller than 0.4 is acquired, one can speak of monodispersed particles with DLS measuring technique.[43] When the diffusion coefficient is calculated, the light distribution can be plotted against size. These sizes are always size ranges and not a single size. Processing data more, or overcalculating, to get volume, mass and number distributions can be done,[46] but it should be noted that initial errors are taken into further calculations to acquire these distributions. Thus different distributions should only be used for comparison or estimations.[39] Z-average, or during this thesis often called hydrodynamic diameter, is a relative consistent parameter and it should always be reported with DLS data. However, Z-average is only accurate for monodisperse samples, and cannot be compared directly with different measurement techniques. It gives an indication of size of spherical particles in solvent. Besides Z-average, light intensity scattering count and light intensity plots can be extracted. When DLS provides a monodisperse signal, indicating micelles are formed, TEM can be performed to identify a more exact size and morphology of the particle. To really prove that micelles are micelles and not vesicles, AFM can be performed.[47] During this thesis stained TEM is performed, since these pictures have a better outline due to increased contrast, but the stain and evaporation of the solvent can influence the result. Thus, to keep the sample less influenced, Cryo-EM is also performed in which the sample is kept in solvent and no stain was added.[48] Due to the polar part of the polymer which stretches in the solvent, extreme low local densities of the carbon backbone result in that part of the micelles will be unseen by TEM. Therefore, the exact size of micelles will be in between the hydrodynamic diameter and the TEM provided size. It should be noted that TEM of something that is not seen, after decomposition, is inaccurate. Only very little part of the sample is investigated with TEM compared to DLS. TEM is not a light intensity distribution measurement but a number distribution measurement. However, when DLS data is transferred to number distribution they seem very comparable when closed packed particles are used.[49] Concluding that TEM is a proper addition with DLS for micelles decomposition but not to many conclusions can be made from it.

Fluorescence is very sensitive compared to UV-absorption and ^{1}H-NMR for observing low concentrations in solution, making it ideal for tracing low concentration of (model) drug release. Nile red (NR) is a model drug, which fluorescence fades away in water and is only fluorescence in hydrophobic environment. [50] Excitation at 540 nm and emission can be traced with a maximum at 633 nm.[51] Difference in the maximum of excitation correlates to the amount of NR released.[52] Drug loading can be determined by making a calibration curve in DMF, micelles decompose fully in DMF and NR is fluorescent in DMF.[51] Doxorubicin is also a fluorescent drug and functions by inhibiting Toipoisormerase.[32] During this

thesis the Doxorubicin•HCl is made hydrophobic (DOX), favoring drug loading in the hydrophobic core micelles. Drug loading and drug release is investigated by fluorescence, DOX is soluble and thus fluorescent both in water as in micelles making the drug release more complicated to track.[53] DOX is more fluorescent in hydrophobic environment and less in water. When DOX is too concentrated, it can aggregate, especially when the hydrophobic DOX is used. In aggregated state DOX is expected to be less fluorescent, due to quenching. During this thesis, two methods are used to observe DOX drug release. First with dialysis, where the micelles are separated from released DOX. Secondly without dialysis, where the micelles with loaded DOX is observed. DOX can be excited with a wavelength of 490 nm and can be traced with a maximum in fluorescence at 590nm.[54] Beside difficulty in fluorescence, literature describes that DOX is sensitive to environment and can become less fluorescent when temperature is increased or when H_2O_2 is added.[55]

Previous work

This thesis will continue on previous research conducted mainly by L. Reinalda.[56] During this previous research project, three block copolymer PD_XM_Y were synthesized and tested as a drug delivery system. In this project, two previously synthesized block copolymers PD_XM_Y have been studied. One contains 130 N,N- dimethylacrylamide (DMA) groups and 16 4-(methylthio)phenyl acrylate (MTPA) groups ($PD_{130}M_{16}$), whereas the other block copolymer contains 85 DMA groups and 26 MTPA groups ($PD_{85}M_{26}$). In further experimental work both $PD_{130}M_{16}$ and $PD_{85}M_{26}$ are referred to with the generic term PD_XM_Y, meaning that the experiment was performed with both polymers separately. MTPA as hydrophobic part in the polymer chain can be used as a trigger for drug release with H_2O_2 addition. The MTPA block in the polymer is nonpolar, however, by oxidizing and hydrolyzing at the MTPA block of the polymer, this block becomes polar instead of nonpolar, which makes the entire polymer soluble in aqueous condition. The first steps in drug loading and drug release including the interaction of these micelles with H_2O_2 were also performed and will be repeated and continued in this work.

Research goals

The main goal of this thesis is to establish a drug delivery system based on PD_xM_Y micelles which are sensitive to ROS. To prove the formation of micelles and to give an indication about their size and stability, ^{1}H-NMR, DLS, TEM and Cryo-EM measurements were performed over longer time spans.

The interaction of PD_XM_Y micelles with ROS was investigated by using H_2O_2 addition. For visibility of decomposition of the micelles core (consisting of MTPA blocks), ^{1}H-NMR and DLS measurements were performed. In addition, PD_XM_Y micelles interaction with H_2O_2 was investigated by TEM and Cryo-EM.

Drug loading and drug release was investigated by addition of NR to PD_XM_Y micelles. NR functions as a model drug, due to its hydrophobicity and fluorescence. After incubation, the drug release is investigated by fluorescence after addition of H_2O_2. In addition, the drug release of DOX was investigated by fluorescence. Due to the fluorescence of DOX in both water and micelles, visualizing DOX drug release is more challenging to quantify.

To finalize this project, it was investigated whether gamma radiation induces sufficient ROS to oxidize MTPA groups in micelles. In addition, the required dose of gamma radiation would still induce a physical change in morphology of the micelles was investigated by DLS. The drug loaded micelles with gamma radiation were observed by fluorescence. In Fig 2.4 a scheme is provided, with the proposed mechanism during this thesis.

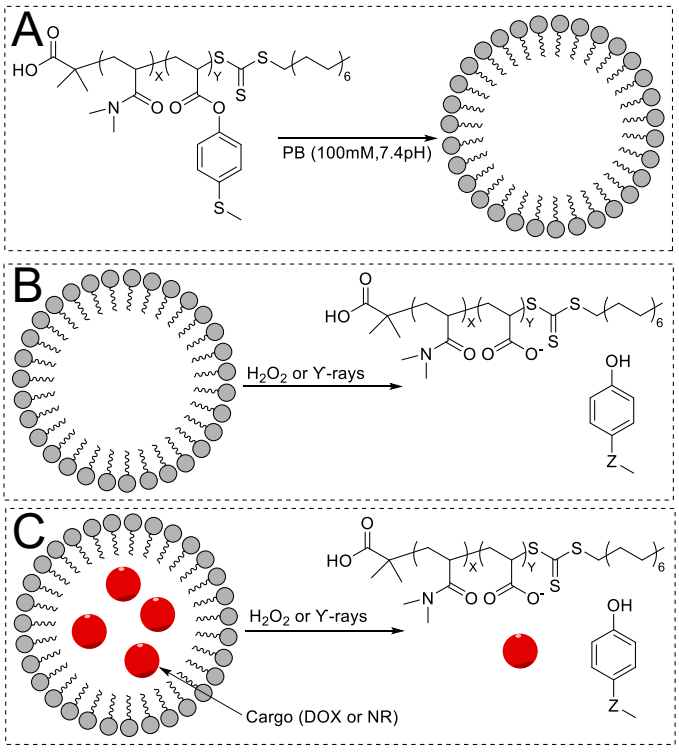

Fig(2.4) Adjusted figure from.[56] Proposed scheme of project overview A; The expected micelle formation, after dissolving PD_XM_Y in aqueous conditions. B; Proposed scheme of micelle decomposition, by H_2O_2 addition or by gamma radiation. C; Proposed scheme of drug release, by H_2O_2 addition or by gamma radiation.

Method and materials

Method

Micelles formation

Syntheses of PD_XM_Y micelles in PB (*General Procedure PB*). 10 mg PD_XM_Y was dissolved in around 300 up to 400 µl THF. Dropwise 10 ml of Phosphate based buffer (100mM, pH7.4) (PB) was added, giving a solution of 1 mg/ml. The mixture was stirred overnight to let the THF evaporate at R.T.

Syntheses of PD_XM_Y micelles in HEPES (*General Procedure HEPES*).10 mg PD_XM_Y was dissolved in around 300 up to 400 µl THF. Dropwise 10 ml of HEPES buffer (100mM, pH7.4), was added, giving a solution of 1 mg/ml. The mixture was stirred overnight to let the THF evaporate at R.T.

Micelles behavior at different environment

PD_XM_Y micelles behavior at elevated temperatures, NR loaded DLS. PD_XM_Y micelles were made according to *General Procedure PB* and were exposed at R.T. and to 37°C whilst being loaded with NR and unloaded (See *loading PD_XM_Y micelles with NR*). Before DLS measurement the mixture was filtered by a 0.45 µm syringe filter. DLS measurements were performed over a few days up to weeks.

DLS of PD_XM_Y micelles during H_2O_2 addition. PD_XM_Y micelles were made according to *General Procedure PB*. All the experiments were performed at 37°C. Before addition of H_2O_2 the 1 ml PD_XM_Y solution was filtered by a 0.45 µm syringe filter. PD_XM_Y micelles were exposed to 0 wt%, 2 wt%, 0.2 wt% and 0.007 wt% H_2O_2 additions. By adding, to a 1 ml PD_XM_Y solution, 66 µl H_2O_2 (30 wt%) resulting in a 2 wt% H_2O_2 concentration overall. By adding to a 1 ml PD_XM_Y solution 66 µl H_2O_2 (3 wt%) resulting in a 0.2 wt% H_2O_2 concentration overall. By adding, to a 1 ml PD_XM_Y solution, 26 µl H_2O_2 (0.3 wt%) resulting in a 0.007 wt% H_2O_2 concentration overall. By adding, to a 1 ml PD_XM_Y solution, no H_2O_2 resulting in a 0 wt% H_2O_2 concentration overall. These 8 samples were held in a bath of 37°C during the measurements and observed up to 11 days.

Stained TEM of PD_XM_Y micelles before and after 2 wt% H_2O_2 addition. Four samples of 1 ml PD_XM_Y micelles were made according to *General Procedure PB*: $PD_{130}M_{16}$ 0 wt% H_2O_2, $PD_{130}M_{16}$ 2 wt% H_2O_2, $PD_{85}M_{26}$ 0wt% H_2O_2 and $PD_{85}M_{26}$ 2 wt% H_2O_2. After 48 hours the samples were prepared for TEM by adding a few µl PD_XM_Y micelles solution on a cupper grid with carbon film in between the grids, the grid was washed and dried 3 times with water and paper. Lastly a few µl Uranyl (2 wt%) was pipetted on the grid and dried. After drying the TEM pictures were made.

Cryo-EM of PD_XM_Y micelles before, during and after 0.2 wt% H_2O_2 addition. 6 samples of 2 ml PD_XM_Y micelles were made according to *General Procedure PB*. Two samples of 0.2 wt% H_2O_2 $PD_{130}M_{16}$ were prepared by adding 132 µl H_2O_2 (3 wt%) to 2 ml of the micellar dispersion and measured after 12 and 24 h. Two samples of 0.2 wt% H_2O_2 $PD_{85}M_{26}$ were prepared by adding 132 µl H_2O_2 (3 wt%) to 2 ml of the micellar dispersion and measured after 24 and 40 h. 2 ml $PD_{130}M_{16}$ with no addition of H_2O_2 was prepared. And 2ml $PD_{85}M_{26}$ with no addition of H_2O_2 was prepared. These 6 samples were inserted in six centrifuge filters (10 kDa). These filters were centrifuged 15 min at 4,000 RPM, the six samples were concentrated to around 20 mg/ml. The 100 µl was extracted from the filters and washed with 100 µl water. Samples of around 10mg/ml were provided for Cryo-EM.

^{1}H-NMR $PD_{85}M_{26}$ polymer before and after 2 wt% H_2O_2. Three samples were prepared for ^{1}H-NMR (*400MHz DMSO*):

- 5 mg $PD_{85}M_{26}$ micelles were made according to *General Procedure PB*. 0.33 ml H_2O_2 (30 wt%) was added to 5 ml $PD_{85}M_{26}$ micelles. After 24 h, the samples solvent was removed using a rotary evaporator at 43°C until the sample was completely dry. 500 µl deuterated DMSO was added and filtered by a 0.45 µm syringe filter.
- 5 mg $PD_{85}M_{26}$ polymer was dissolved in 500 µl deuterated DMSO.
- 5 mg 4-(Methyl sulfonyl)phenol was dissolved in 500 µl deuterated DMSO.

^{1}H-NMR of PD_XM_Y micelles after H_2O_2 addition in PB/D_2O 9:1 mixture. Seven samples were prepared for ^{1}H-NMR (*400MHz D2O*):

2 ml PD_XM_Y solution was made according to *General Procedure PB* with a final concentration of 4 mg/ml instead of 1 mg/ml. 0.5 ml PD_XM_Y micelles (4 mg/ml) solution was taken and 55µl D_2O was added, in an NMR tube. 33 µl H_2O_2 (30 wt%) was added to the NMR tube and every hour a measurement was taken.

Likewise, an NMR was prepared for 4-(methylsulfonyl)phenol, 4-(methylsulfinyl)phenol, 4-(methylthio)phenol and PD_XM_Y with no H_2O_2 addition in a D_2O/PB (1:9) mixture.

Micelles drug loading

Loading PD_XM_Y micelles with NR. 2 mg Nile red (NR) was dissolved in 2 ml THF, forming a 1 mg/ml NR solution. 20 µl NR solution was added to 1 ml PD_XM_Y micelles made according to *General Procedure PB*. The PD_XM_Y NR solution was stirred overnight to evaporate the THF. Afterwards, the sample was incubated at 37°C for 1 day. The sample was used within 2 days, because NR degrades over time. The entire process was performed as much as possible in a dark environment.

Loading PD_XM_Y micelles with DOX[57]. 50 µl Doxorubicin•HCl DMSO (100 mg/ml) solution and 1.8µl (1.5 mol equivalent) Triethylamine was mixed in 200 µl DMF. 10 mg PD_XM_Y was dissolved in 300 µl DMF. The two solutions were mixed and stirred for 6 hours at 35°C in the dark. Then dropwise, 10 ml PB was added and stirred overnight. Dialysis bags with a pore size of 14 kDa were used, the 10 ml solution was added into the dialysis bag. A beaker of 2 liter was used and the water was refreshed up to 2 times a day for 3 up to 4 days. After 4 days the solution, within the dialysis bag, was freeze dried. Dropwise, 10 ml PB was added. The solution was filtered with a 0.45 µm syringe filter. DOX loaded micelles were obtained in PB. The entire process was performed as much as possible in a dark environment.

Drug loading efficiency

Drug loading test with model drug NR. A stock solution of 1 mg/ml NR in PB/DMF mixture (1:9) was made. The stock solution was diluted in 10 steps to 0.0001 mg/ml. And fluorescence was used to determine intensity maximum at 633nm of NR. Next 1 ml of PD_XM_Y micelles with NR according to *loading PD_XM_Y micelles with NR* were used and centrifuged at 5,000 rpm for 10 min. A red precipitate was observed at the bottom of the vial. 900 µl of the solution was removed and refilled with PB, this was repeated 3 times. Next, again, 900 µl was extracted and 900 µl DMF was added. The PD_XM_Y micelles with NR were completely dissolved in PB/DMF mixture (1:9).

Drug release

Drug release test with model drug NR. 26.4 µl H_2O_2 (30 wt%) was added to 0.4 ml PD_XM_Y micelles loaded with NR solution according to *loading PD_XM_Y micelles with NR* resulting in a 2w% H_2O_2 solution. 26.4 µliter H_2O_2 (3 wt%) was added to 0.4 ml PD_XM_Y micelles loaded with NR solution according to *loading PD_XM_Y micelles with NR* resulting in a 0.2 wt% H_2O_2 solution. 8.7 µliter H_2O_2 (0.3 wt%) was added to 0.4 ml PD_XM_Y micelles loaded with NR solution according to *loading PD_XM_Y micelles with NR* resulting in a 0.007 wt% H_2O_2 solution. Fluorescence was traced by the Biotek microplate reader, which was kept at 37°C. NR was excited at 540 nm and emission was measured every 30 min for 72 hours at wavelengths of 620 nm, 633 nm, and 645 nm automatically. The wells were filled with 250 µl solution with the previous 6 described samples plus 2 samples with no H_2O_2 addition. The emission was measured at 37°C and at 25°C. The entire process was performed as much as possible in a dark environment.

Fluorescence DOX with dialysis bag. 4 ml PD_XM_Y micelles with DOX were made according to Loading PD_XM_Y micelles with DOX. 2 ml PD_XM_Y micelles were loaded within a 14 kDa dialysis bag. The bag was submerged in a mixture of 300 ml PB with 19.8 ml H_2O_2 (30 wt%). The fluorescence of the surroundings was measured by extracting 1 up to 3 ml (depending on the volume of the cuvette for the measurement) of the surroundings at excitation wavelength of 490 nm and at emission wavelength of 590 nm. Same process was performed without addition of H_2O_2 as a control measurement. Note, accumulation of red particles at the dialysis bag was observed. The entire process was performed as much as possible in a dark environment at 37°C.

Fluorescence DOX without dialysis bag. $PD_{130}M_{16}$ micelles loaded with DOX made according to *loading PD_XM_Y micelles with DOX*. 0.2 ml of $PD_{130}M_{16}$ micelles with DOX was diluted 150 times by addition of 30ml PB. Four samples were made:

- 196 µl H_2O_2 (30 wt%) was added to 3 ml of the diluted $PD_{130}M_{16}$ micelles with DOX after 96 hours and was measured over time by fluorescence. Representing 2 wt% H_2O_2 addition.
- 19.6 µl H_2O_2 (30 wt%) was added to 3 ml of the diluted $PD_{130}M_{16}$ micelles with DOX after 96 hours and was measured over time by fluorescence. Representing 0.2 wt% H_2O_2 addition.
- 6.6 µl H_2O_2 (3 wt%) was added to 3 ml of the diluted $PD_{130}M_{16}$ micelles with DOX after 96 hours and was measured over time by fluorescence. Representing 0.007 wt% H_2O_2 addition.
- And one control with no addition of H_2O_2 to 3 ml of the diluted $PD_{130}M_{16}$ micelles with DOX and was measured over time by fluorescence. Representing 0 wt% H_2O_2 addition.

The samples were excited at 490 nm and emission maximum at 590 nm was traced at R.T. the entire process was kept in the dark.

Fluorescence DOX without dialysis bag without PDXMY. 75 µl of a solution of Doxorubicin•HCl in DMSO (100 mg/ml) and 2.7µl (1.5 mol equivalent) Triethylamine was mixed in 300 µl DMF. The solution was stirred overnight in the dark at elevated temperature of 37°C. Dropwise, 15 ml PB was added to the mixture. The solution was stirred overnight at 37°C. 0.2 ml was extracted and diluted 150 times by addition of 30 ml PB. After 96 hours, 196 µl H_2O_2 (30 wt%) was added to 3 ml of the solution, resulting in 2 wt% H_2O_2 addition.

The fluorescence was measured over time and the sample was excited at 490 nm and emission maximum at 590 nm was traced at R.T.

Micelles exposed to ionizing radiation

Micelles in PB exposed to different dose gamma rays. Three 1 ml $PD_{130}M_{16}$ samples and three 1 ml $PD_{85}M_{26}$ samples were made according to *General Procedure PB*. The six samples were inserted in the 220 ^{60}Co source. After a dose of 67 Gy 1 sample of $PD_{130}M_{16}$ and one sample of $PD_{85}M_{26}$ was extracted. After a dose of 120 Gy one sample of $PD_{130}M_{16}$ and one sample of $PD_{85}M_{26}$ was extracted. After a dose of 500 Gy one sample of $PD_{130}M_{16}$ and one sample of $PD_{85}M_{26}$ was extracted. These six samples were over a time span up to 15 days observed by DLS.

Micelles in HEPES exposed to different dose of gamma rays. Three 1ml $PD_{130}M_{16}$ samples and three 1 ml (1mg/ml) $PD_{85}M_{26}$ samples were made according to *General Procedure HEPES*. The six samples were inserted in the 220 ^{60}Co source. After a dose of 82 Gy one sample of $PD_{130}M_{16}$ and one sample of $PD_{85}M_{26}$ was extracted. After a dose of 120 Gy one sample of $PD_{130}M_{16}$ and one sample of $PD_{85}M_{26}$ was extracted. After a dose of 500 Gy one sample of $PD_{130}M_{16}$ and one sample of $PD_{85}M_{26}$ was extracted. These six samples were over a time span up to three days observed by DLS.

GPC in THF (size exclusion). 1mg of PD_XM_Y was dissolved in 1ml THF. 50 µl was loaded in the GPC, the UV absorption at 254nm was measured and the RI was measured.

GPC in THF exposed to gamma rays (500 Gy) (size exclusion). 5 ml of $PD_{130}M_{16}$ solution was made according to *General Procedure PB*. The $PD_{130}M_{16}$ solution was radiated in 220 ^{60}Co source with 500 Gy. After radiation, the sample was freeze dried overnight, and 5 ml THF was added to the $PD_{130}M_{16}$ radiated polymer. The Phosphate salts were filtered by a 0.45 µm syringe filter. 50 µl solution was loaded in the GPC, the UV absorption at 254 nm was measured and the RI was measured.

^{1}H-NMR of PDXMY micelles exposed to gamma rays. 2 ml PD_XM_Y micelles solution was made according to *General Procedure PB*, instead of 1mg/ml the concentration was raised to 4 mg/ml. 0.5 ml was transferred into a vile and irradiated with 500 Gy in the 220 ^{60}Co source. The sample was transferred into an NMR tube and 55µl D_2O was added. Right after radiation and 24 hours after radiation a ^{1}H-NMR measurement was performed.

Radiolabeling.1 ml $PD_{85}M_{26}$ micelles was provided according to *General Procedure HEPES*. Where 50 kBq (~5uL, in HCl pH 2) of In-111 was added to the $PD_{85}M_{26}$ micelles and stirred for 1 hour. The sample was separated by size exclusion chromatography.

Materials

Chemicals

PD_XM_Y polymers were obtained from previous research conducted by L. Reinalda and I. Piergentilli.[56] All solvents and reagents were from Sigma Aldrich, TCl Chemicals or Acros Organics.

Devices

^{1}H-NMR spectra were recorded at 400 MHz with the Agilent-400 MR DD2.

The Shimadzu GPC was equipped with UV-absorption at 254nm and a refractive index detector, with a THF column.

Three fluorescence devices were used during this thesis.

- The Jasco J-815 CD spectrometer was used for drug loading measurement of Nile Red.
- The Biotek Synergy H1 microplate reader was used for drug release experiments of Nile Red.
- The SPEX fluorimeter was used for all DOX related fluorescence measurements.

The Zetasizer Nano ZS was used for all DLS measurements with 633 nm laser at with a detector angle of 173.5 detector.

The Gammacel 220 of Reactor Institute Delft was used for gamma radiation during 6-2020 up to 12-2020.

JEOL JEM-1400 plus was used for TEM and Cryo-EM pictures.

Results and discussion

Micelles characterization (determined by DLS, TEM, Cryo-EM measurements)

To establish micelles made from $PD_{130}M_{16}$ and $PD_{85}M_{26}$ block copolymers, the interaction between PD_XM_Y and PB (100 mM pH 7.4) was investigated. To this end, PD_XM_Y (1 mg/mL) was exposed to PB at R.T., light intensity scattering and hydrodynamic diameter were measured by DLS. From these measurements, it was observed that $PD_{130}M_{16}$ solution has a light intensity scattering around 2,000 kcps constantly over time with a hydrodynamic diameter of around 30 nm and only one single peak in the light intensity distribution (Fig 4.1 A). This sharp peak combined with the PDI between 0.15 and 0.4 provided by the DLS indicate that monodisperse particles were produced.[43] For $PD_{85}M_{26}$ in PB solution light intensity scattering around 15,000 up to 25,000 kcps was observed with a hydrodynamic diameter between 50 and 60 nm (Fig 4.1 B, C). When repeating this experiment, different batches gave more stable light intensity scattering as shown later in report (Fig 4.7). The observed increase in light intensity scattering of $PD_{85}M_{26}$ in PB solution could be caused by the formation of new particles or due to big particles disturbing scattering rate. Also, a small second and very small third peak were observed for $PD_{85}M_{26}$ in PB solution in the light intensity distribution indicating that not only monodisperse particles were produced but also a few bigger particles (Fig 4.1A). In addition, it should be noted that the exact size of particles is inaccurately determined by DLS, since DLS only measures if a particle is in between two sizes (for example the size of the particle is between 32 and 37 nm) and not a single value for the size. Besides that, DLS makes few assumptions for correlating particle size to light distribution.[58] However, in the light intensity distribution, a dominant peak at 30 nm for $PD_{130}M_{16}$ and 50 nm for $PD_{85}M_{26}$ was observed, indicating that mainly monodisperse particles are formed. For both $PD_{130}M_{16}$ and $PD_{85}M_{26}$, it can be concluded that after addition of PD_XM_Y to PB, rather monodisperse structures are produced which give a strong indication that micelles are formed.

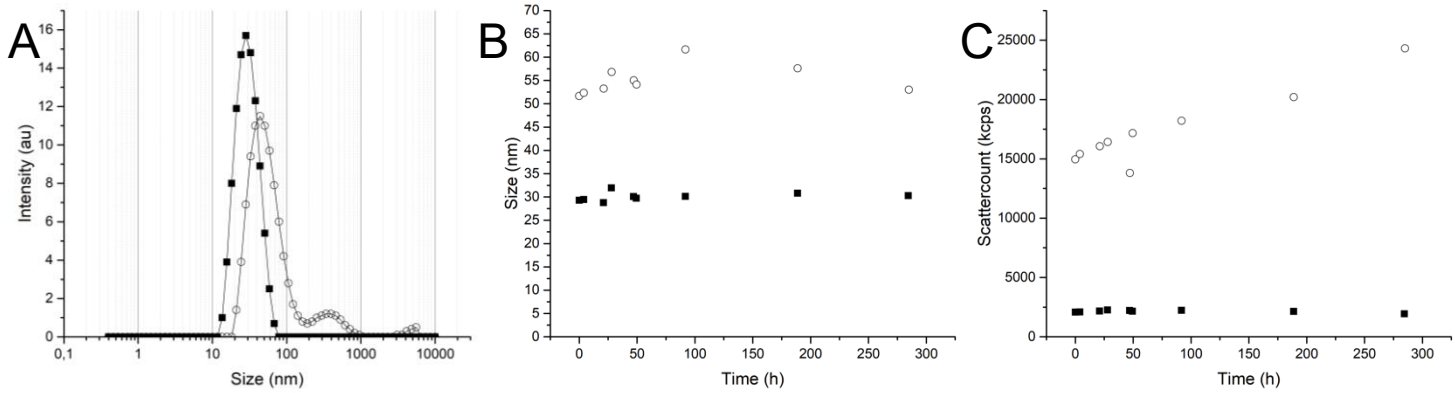

Fig (4.1) (○=$PD_{85}MTPA_{26}$; ■=$PD_{130}M_{16}$) A; Initial light intensity plot for $PD_{85}M_{26}$ and $PD_{130}M_{16}$, maximum of main peaks equals the Z-average, a slight second bump causes uncertainty for $PD_{85}M_{26}$ for scattering and Z-average. B; Z-average for $PD_{85}M_{26}$ and $PD_{130}M_{16}$ over 11 days, size for $PD_{85}M_{26}$ is around 50nm, size for $PD_{130}M_{16}$ is around 30 nm. C; Normalized light intensity scattering for $PD_{85}M_{26}$ and $PD_{130}M_{16}$ over 11 days, $PD_{130}M_{16}$ forms smaller particles thus less light intensity scattering compared with $PD_{85}M_{26}$, $PD_{85}M_{26}$ increase in scattering caused by slight formation of bigger particles over time.

To prove that the structures observed by DLS are micelles, $PD_{130}M_{16}$ and $PD_{85}M_{26}$ in PB were made, the solutions were further studied by TEM. Due to the polarity of the stain, the uranyl will attach to the DMA part of the polymer which is used to visualize the structures. From these measurements, particles with a diameter of 25.8 nm were observed for $PD_{85}M_{26}$ and particles of 16.8 nm diameter for $PD_{130}M_{16}$ (Fig 4.2 A, B). The difference in size could be explained by a difference in the MTPA block length of the polymer chain. Since it is expected that $PD_{85}M_{26}$ (containing 26 MTPA groups) will have a bigger core compared to the core of $PD_{130}M_{16}$ (with only 16 MTPA groups), the size difference is thus explained by steric hindrance. The boundary of the micelles, consisting of the DMA block, prefers interaction with the uranyl stain after evaporation of the solvent. This causes a sharp line around the hydrophobic MTPA core. After evaporation of the solvent the DMA/uranyl local mixture prefers to minimize surface tension and become concise leading to narrow ring around the core. However, these results will not give a certain indication of the assembly's morphology in solution. For both $PD_{130}M_{16}$ and $PD_{85}M_{26}$ in PB, TEM does not give an indication how the micelles look like in solution. This is due to the fact, that the solution around the micelles is evaporated and stain is added. First, due to evaporation of solvent resulting in locally high concentrations of micelles in solvent, which can change the morphology of the structures. Secondly, the stain is an extra variable, which can also result in a change of the morphology of the structures. To visualize the structures in solution and to prevent evaporation of solvent or using a stain, Cryo-EM could be used as additional technique. Cryo-EM does not

evaporate the solution but instead freezes it, while no stain is used to keep the structures fixed on the grid (since the structures will be frozen). Therefore, Cryo-EM could be a valuable technique to further investigate the observed structures.

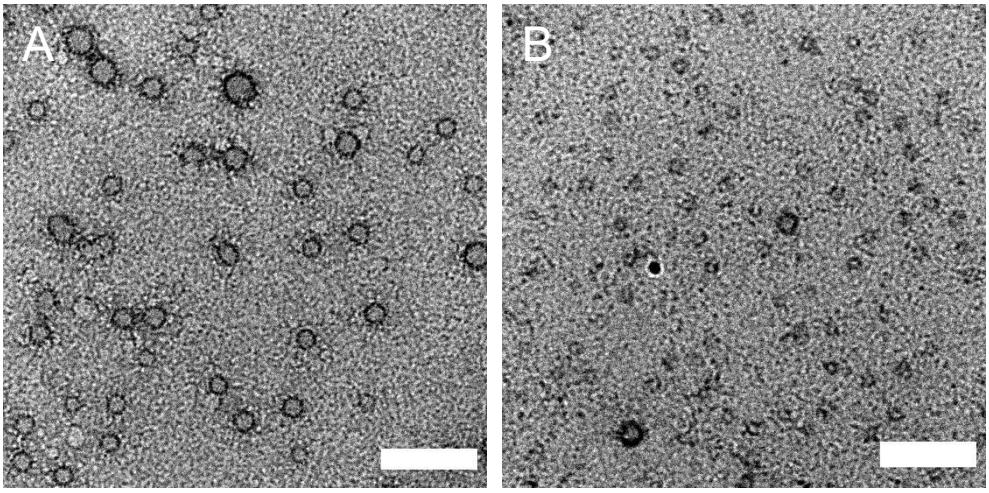

Fig (4.2) Scalebar=100nm A; TEM, stained with 2 wt% Uranyl, of $PD_{85}M_{26}$ in PB show spherical particles stain accumulates mostly at the boundary giving indication micelles are formed. Average diameter is 25.8 nm based on ~20 particles. B; TEM, stained with 2 wt% Uranyl, of $PD_{130}M_{16}$ in PB show spherical particles with slightly darker boundary. Average diameter 16.8 nm based on ~20 particles.

To prove that structures previously observed by TEM are micelles, $PD_{130}M_{16}$ and $PD_{85}M_{26}$ in PB were prepared according to *general procedure PB* and investigated by Cryo-EM. The polymer solutions were added on Cryo-EM grids. In these grids are holes, where a very thin layer of solution will freeze, the solvent within these holes is where the Cryo-EM pictures are made from. To ensure particles are visible in this very thin film, 1 mg/ml solution is centrifuged with 10 kDa filters to get a final concentration of ~10 mg/ml. On the Cryo-EM images, spherical particles were observed with a size of 12.4 nm for $PD_{130}M_{16}$ and a size of 23.4 nm for $PD_{85}M_{26}$. The spherical particles had a fading grayness when reaching the boarders (Fig 4.3). This observation was expected from micellar solutions, due to micelles being most dense in the core and becoming less dense at the boundary. Compared to the stained TEM images, the observed structures are less striking due to the absence of stain resulting in less contrast. However, these structures are very "untouched", demonstrating a true representation of the particles in solution. Furthermore, it can be excluded that vesicles are formed, due to the homogeneity of color that is observed in the Cryo-EM images, whereas a double layer with a lighter core was expected to be observed when vesicles would have been formed. Due to the size of ~15 nm and the little contrast, the images are at the limit of the resolution that Cryo-EM can detect. Smaller structures, then the observed structures will not be detected. However, no indication of even smaller structures is expected, based on previous DLS measurements, where no smaller particles were found at the light intensity distribution (Fig 4.1C). Considering size, shapes and previous DLS data, it can be concluded that micelles were formed from both $PD_{85}M_{26}$ and $PD_{130}M_{16}$ in PB, which can be detected by a combination of DLS, Stained TEM and Cryo-EM.

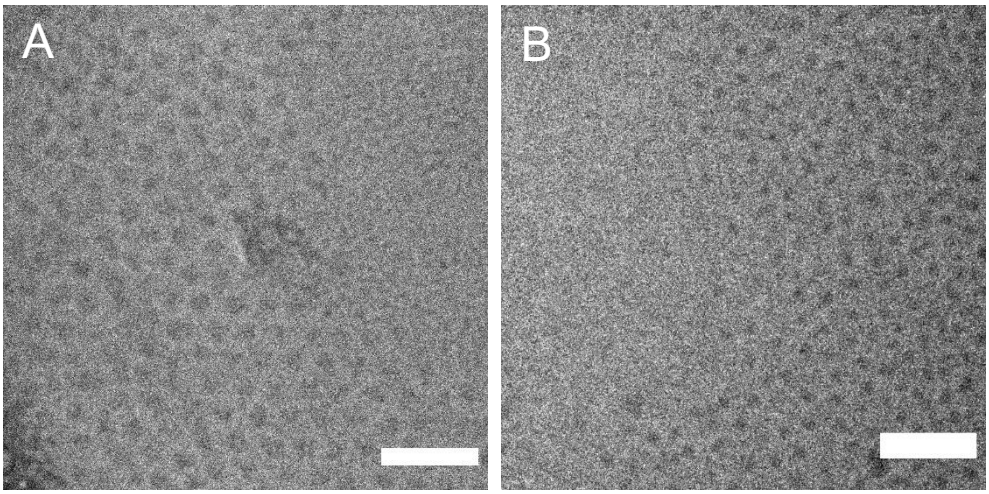

Fig (4.3) Scalebar=100nm A; Cryo-EM of $PD_{85}M_{26}$ particles show spherical particles. Average diameter of 23.5 nm was based on ~20 particles. B; Cryo-EM of $PD_{130}M_{16}$ particles show spherical particles, Average diameter of 12.4 nm based on ~20 particles.

Micelles stability (determined by DLS measurements)

To verify the stability of the PD_XM_Y micelles, DLS measurements of PD_XM_Y micelles in PB were made over time. Both $PD_{130}M_{16}$ and $PD_{85}M_{26}$ micelles were exposed to elevated temperatures up to 37°C and to Nile red (NR), NR is a nonpolar fluorescent molecule which has similar solubility as a nonpolar drug, sometimes in literature described as a model drug.[50] After addition of NR a small increase in size was observed of a few nm over 5 days, this increase is almost insignificant (Fig 4.4). Increasing the temperature from R.T. to 37°C also led to an increase in size of the particles with only a few nm over 5 days. It is shown that $PD_{85}M_{26}$ micelles have a slight second bump in the light intensity plot. (Fig 4.4 B) This could be an indication that $PD_{85}M_{26}$ in PB forms beside micelles also few bigger structures. Nevertheless, still a dominant peak is caused by micelles in the DLS light intensity distribution. Furthermore, in SI 4.1, hydrodynamic diameter and light intensity scattering show that micelles are not significantly affected by the change in temperature or by the NR addition. Thus, PD_XM_Y micelles are still stable after exposure to NR or after increased temperature.

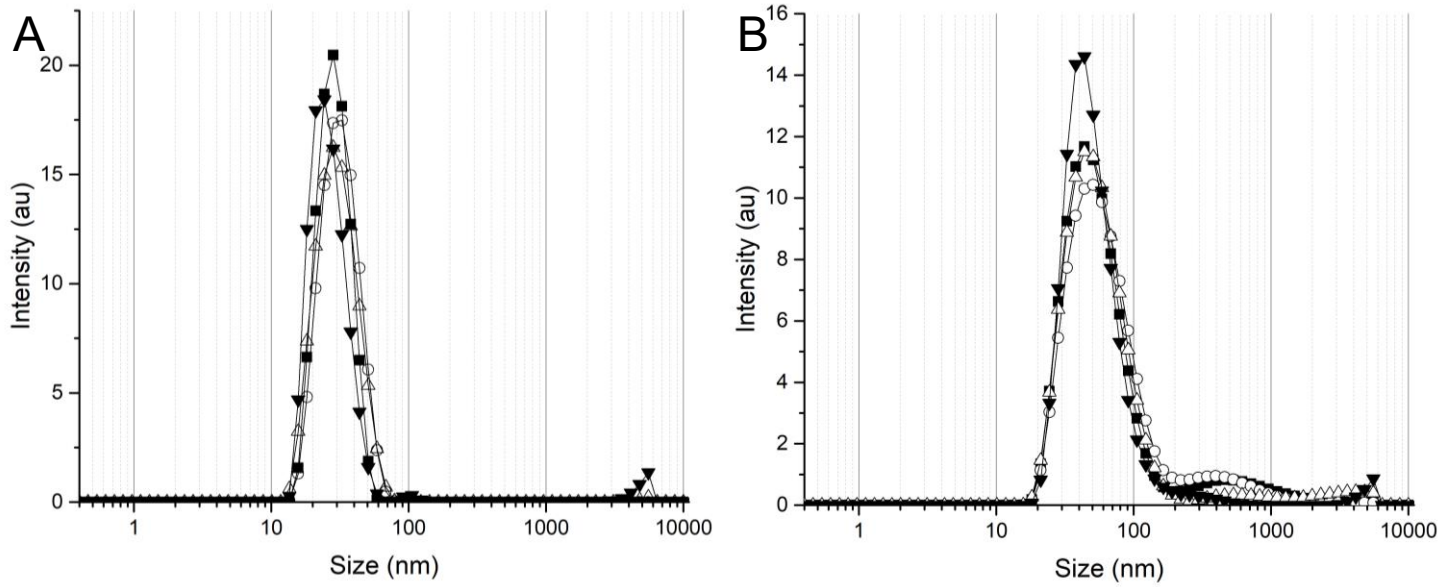

Fig (4.4) (■= T=25C; ○=T=37°C; △=T=25C with NR; ▼=T=37°C with NR) A; Average light intensity plot for $PD_{130}M_{16}$ over 5 days, all variables give similar light intensity plots with maximum at a size around 30 nm. B; Average light intensity plot for $PD_{85}M_{26}$ over 5 days, all variables give similar light intensity plots with maximum at a size around 50 nm with a small bump around a few 100 nm.

Micelles interaction with H_2O_2 (determined by ^{1}H-NMR, DLS, TEM, Cryo-EM measurements)

To investigate how PD_XM_Y polymer will react to addition of hydrogen peroxide (H_2O_2), ^{1}H-NMR are made of: $PD_{85}M_{26}$ in DMSO, of $PD_{85}M_{26}$ in PB with 2 wt% H_2O_2 addition, of 4-(methylsulfonyl)phenol (SO_2Ph) in DMSO and of 4-(methylthio)phenol (SPh) (Fig 4.5). $PD_{85}M_{26}$ is chosen instead of $PD_{130}M_{16}$, because MTPA is more concentrated for $PD_{85}M_{26}$ compared to $PD_{130}M_{16}$, thus $PD_{85}M_{26}$ should be better visible at the MTPA region in ^{1}H-NMR. It is expected that the PD_XM_Y will decompose in SO_2Ph and the polymer backbone (Fig 4.5 A). The chemical shift between 6.5 ppm and 8.0 ppm is defined as the MTPA region. In the $PD_{85}M_{26}$ ^{1}H-NMR, a broad doublet represents the MTPA group and after addition of 2 wt% H_2O_2 these peaks shifted as expected (Fig 4.5 B, C). The formed peaks are in line with SO_2Ph and not in line with SPh (Fig 4.5 D, E). Concluding that SO_2Ph is made after addition of 2 wt% H_2O_2 to $PD_{85}M_{26}$ in PB. However, during this procedure the solutions solvent was removed using a rotary evaporator at 43 °C, this can lead to higher local concentrations and higher temperatures causing different reactions mechanism. Furthermore, it is unknown, if the MTPA group first got oxidized and the hydrolysis reaction happened after, or vice versa. This implicates that maybe initially first SPh is formed or 4-(methylsulfinyl)phenol (SOPh).

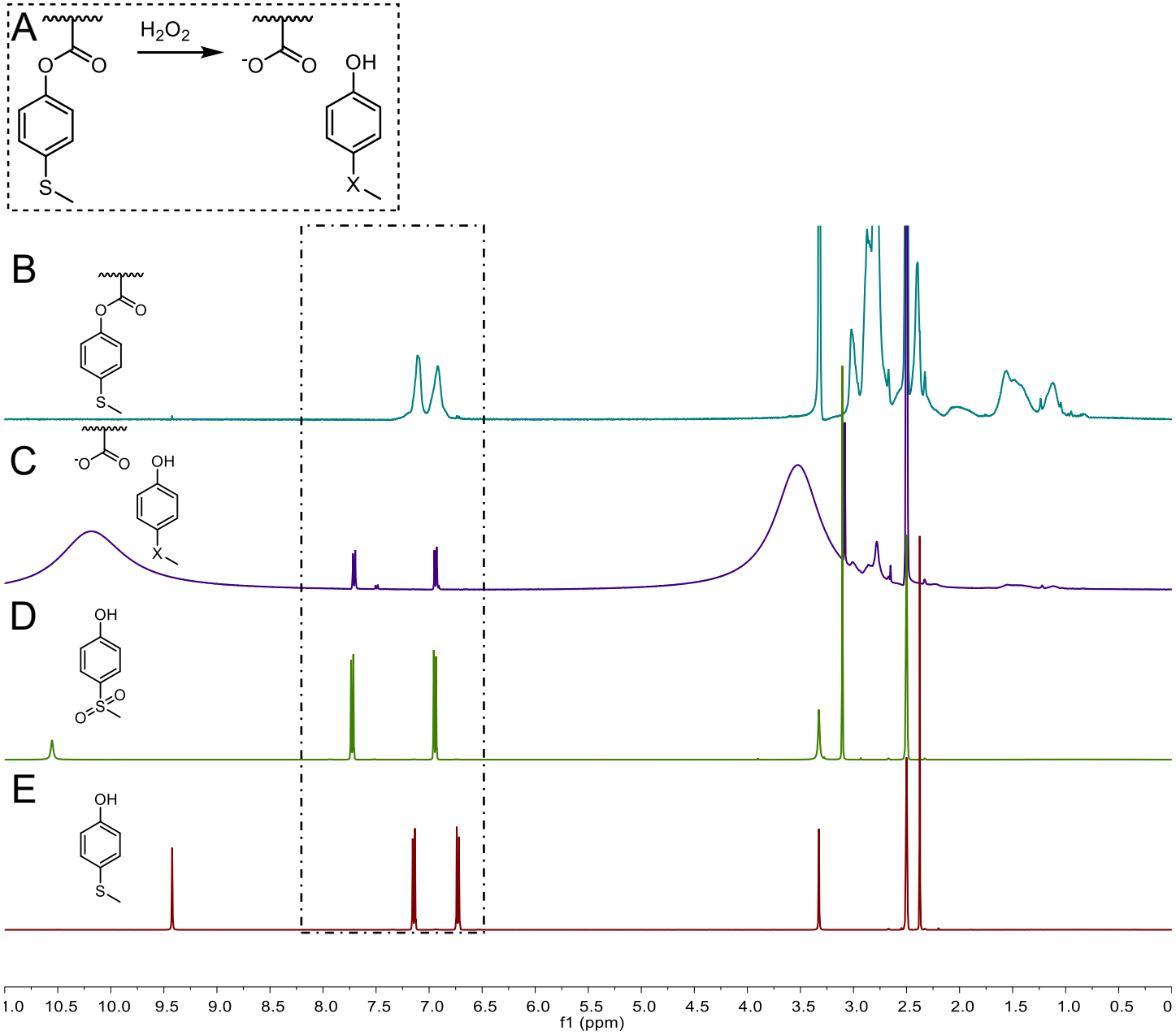

Fig (4.5) ^{1}*H-NMR (400 MHz, DMSO-d6)* A; $PD_{85}M_{26}$ reaction equation with H_2O_2 at, with X representing S, SO or SO2. B; ^{1}H-NMR $PD_{85}M_{26}$ in DMSO. C; ^{1}H-NMR of dried $PD_{85}M_{26}$ after for 48 hours 2 wt% H_2O_2 addition. D; ^{1}H-NMR of SO_2Ph in DMSO. E; ^{1}H-NMR of SPh in DMSO.

To evaluate the decomposition of micelles in time, ^{1}H-NMR was performed. Micelles were made in PB, by addition of PD_XM_Y in PB with 2 wt% H_2O_2 addition. To perform this ^{1}H-NMR experiment the concentration polymer is increased from 1mg/ml to 4mg/ml, otherwise the concentration could be too low for proper visualization, due to potential lack of sensitivity of the ^{1}H-NMR device. Beside increasing the concentration of polymer, D_2O (10 v%) was added for ^{1}H-NMR reference. This PB/ D_2O mixture was directly used for the presaturated ^{1}H-NMR experiment. After addition of 2 wt% H_2O_2 the solution is measured by ^{1}H-NMR over 8 hours. Before addition of H_2O_2 the core of the micelles, the MTPA region, with the aromatic rings is unseen, due to the shielding of the DMA groups (Fig 4.6). After addition of H_2O_2 some sharp peaks start to rise in the aromatic region, between chemical shift 6.0 and 8.0 ppm. According to SI (4.2, 4.3), the main reaction product is SOPh with byproduct SO_2Ph which was previous observed (Fig 4.5). This gives a strong indication that as soon as the sulfur is oxidized once, the hydrolysis reaction happens instead of oxidizing the sulfur twice and then hydrolysis would happen. No hydroxyl peaks are found of the phenol and of the arising acid, which is expected due to the solvents used in the analysis. The reference peaks of D_2O seem to change somewhat making aligning challenging, this could be caused by slight change in pH. Solvent peaks of residual THF at chemical shift of 2.9 ppm, interfere slightly with the spectrum but do not interfere with the MTPA region chemical shift between 8.0 and 6.5 ppm. The main difference between $PD_{130}M_{16}$ and $PD_{85}M_{26}$, is the ratio of MTPA and DMA peaks in the ^{1}H-NMR after addition of H_2O_2 (Fig 4.6). Another difference is the resolution or sharpness of the MTPA region peaks for the $PD_{85}M_{26}$ compared with $PD_{130}M_{16}$ which show more clear peaks, which could be to relative concentration differences of the different polymer blocks. Thus, from this observation we conclude that due to addition by H_2O_2 the core becomes visible and that micelles are decomposing by ejecting mainly SOPh and SO_2Ph.

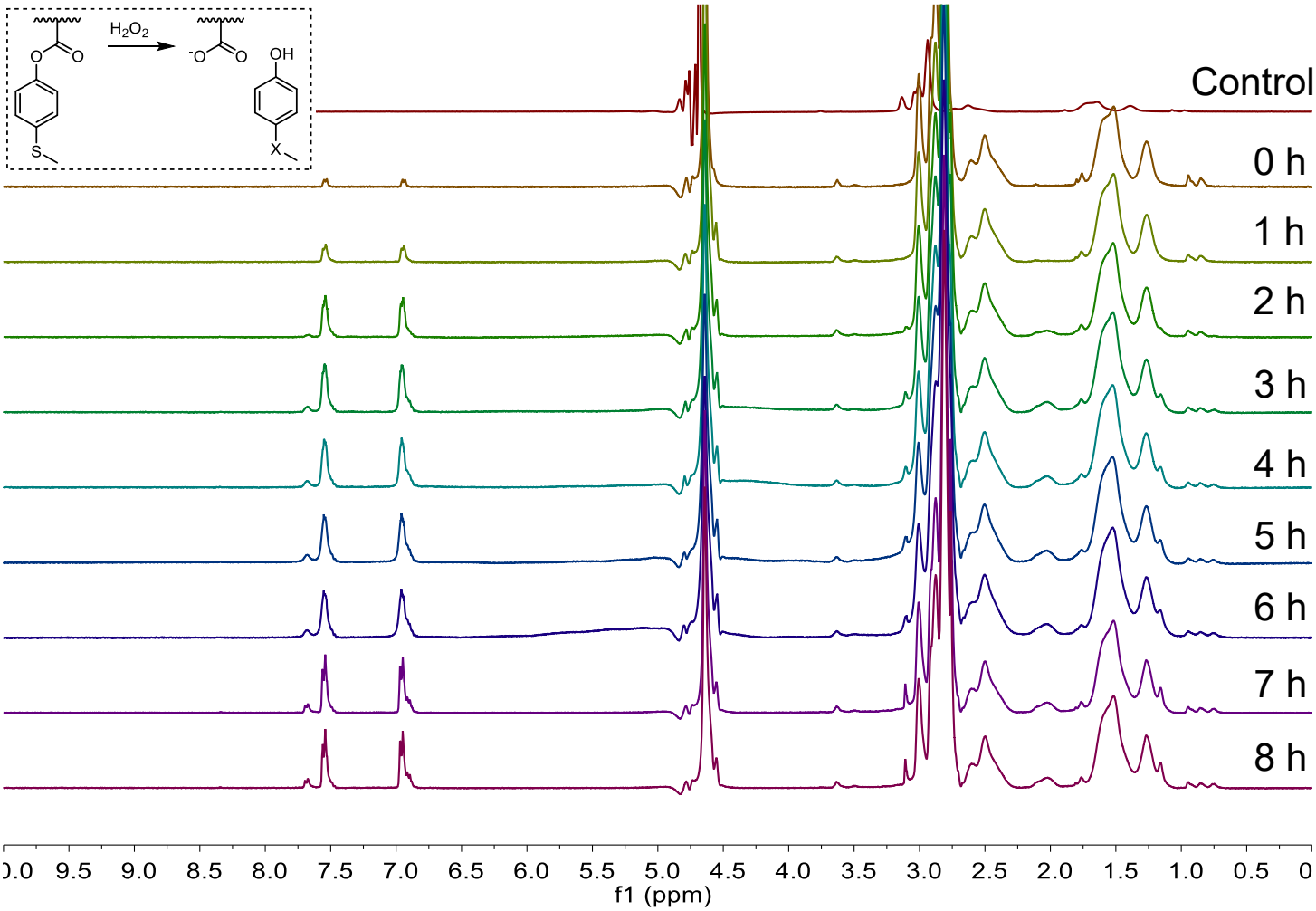

Fig (4.6A) ***^{1}H-NMR (400 MHz, D_2O);*** **Control; ^{1}H-NMR of $PD_{130}M_{16}$ micelles before addition of H_2O_2 in D_2O/PB mixture. 0h-8h; ^{1}H-NMR of $PD_{130}M_{16}$ micelles after addition of 2 wt% H_2O_2 in time steps of around 1 hour. After addition of H_2O_2 the reaction products of the core become visible.**

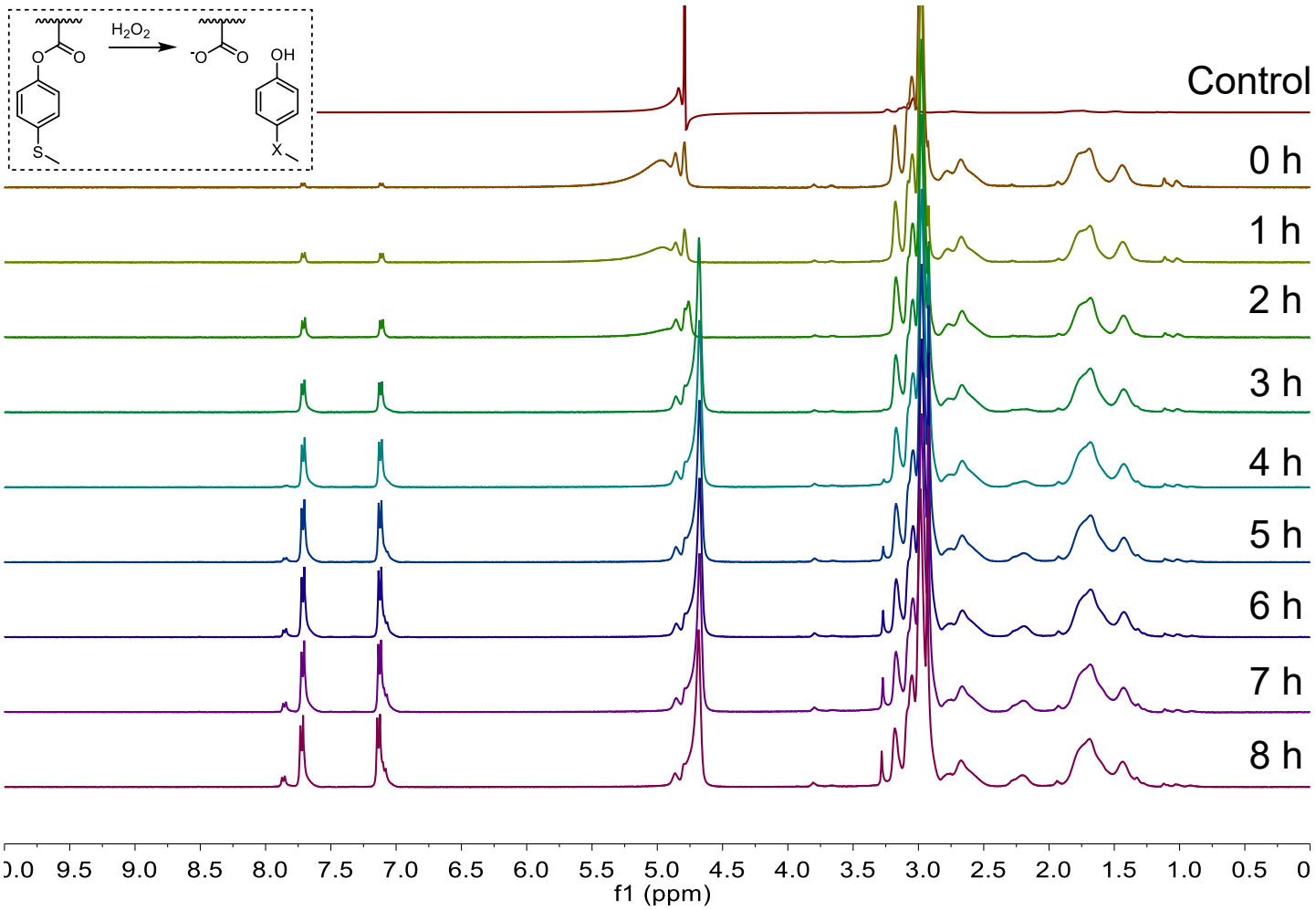

Fig (4.6b) ^{1}*H-NMR (400 MHz, D_2O); Control;* ^{1}H-NMR of $PD_{85}M_{26}$ micelles before addition of H_2O_2 in D_2O/PB mixture. 0h-8h; ^{1}H-NMR of $PD_{85}M_{26}$ micelles after addition of 2 wt% H_2O_2 in time steps of around 1 hour. After addition of H_2O_2 the reaction products of the core become visible.

To demonstrate the morphological change after oxidation and hydrolysis of the micelles, DLS is applied after addition of H_2O_2 and measurements are performed as a function of time. Addition of different fractions between 0.007 wt% up to 2 wt% H_2O_2 with a control measurement (0 wt% H_2O_2) was performed in a period up to two weeks. Change in hydrodynamic diameter and light intensity scattering was observed after addition of H_2O_2 (Fig 4.7). Even 0.007 wt % H_2O_2 leads to change of light intensity scattering for both $PD_{130}M_{16}$ and $PD_{85}M_{26}$ and change in hydrodynamic diameter for $PD_{130}M_{16}$ was observed. The difference in reaction time between $PD_{130}M_{16}$ and $PD_{85}M_{26}$ after 0.007 wt% addition could be explained by the fact that: $PD_{130}M_{16}$ has a lower concentration of MTPA groups compared to $PD_{85}M_{26}$, due to better accessibility of H_2O_2 to the MTPA core of the micelles or due to weaker polymer interaction in the core making a change in size easier. Initially, was expected that when micelles decompose the particle size should become smaller, however, the observation is that the Z-average increases instead. One should recall that, when the small particles in the size distribution disappear the scattering will be dominated by the remaining particles. Nonetheless, the increase in Z-average can also be caused by backbones clustering together forming few bigger structures, this after the oxidation and hydrolysis of the initial micelles. For the $PD_{130}M_{16}$ the amount of light intensity scattering drops and increases in time (Fig 4.7 B). This means that bigger particles are formed after H_2O_2 addition this is: by chemical route due to forming bigger particles or by physical route due to clustering of micelles. The same experiment is performed twice and similar behavior is observed (SI 4.4; 4.5). A possible explanation for this phenomenon is that initially, many micelles decompose after addition of H_2O_2 and dissolve. Afterwards the dissolved polymer backbone gets attracted to each other, which maybe forms unstructured big aggregates. The increase in hydrodynamic diameter is also observed for $PD_{85}M_{26}$, however, the light scattering count decreases, concluding only very few big particles are present (Fig 4.7 C, D). Overall micelles change in morphology after the addition of H_2O_2, the decrease of the number of particles in solution indicate that these PD_XM_Y micelles could be used for drug release with a H_2O_2 trigger.

To visualize the decomposition of micelles and get a better grasp on the bigger particles that are eventually formed, TEM is performed.

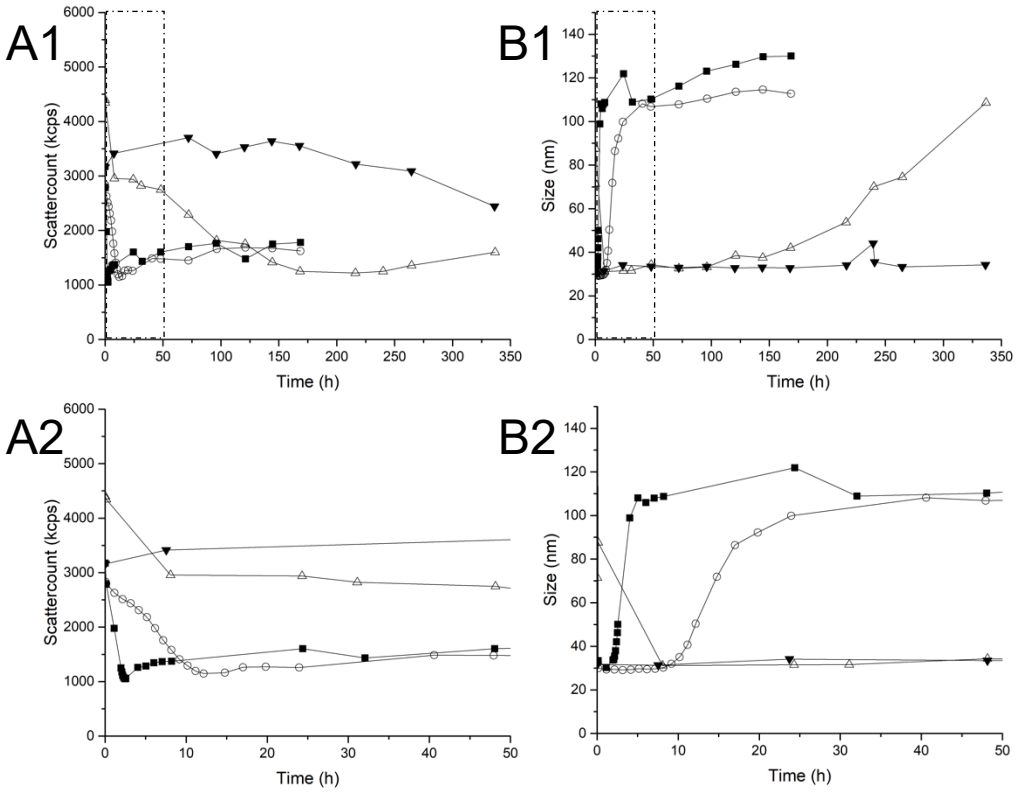

Fig (4.7) (■=2 wt% H_2O_2; ○=0.2 wt% H_2O_2; △=0.007 wt% H_2O_2; ▼=Control (0 wt% H_2O_2) A1; Normalized light intensity scattering of $PD_{130}M_{16}$ in PB after addition of H_2O_2. A decrease in light intensity scattering was observed for all H_2O_2 additions, and within time an increase in light intensity scattering was observed for all H_2O_2 additions. A2; Zoom on A1, to improve the visualization of 2wt% H_2O_2 scattering decrease and increase. B1; Z-average for $PD_{130}M_{16}$ after addition of H_2O_2, initial size around 30nm which increases up to 120 nm over time depending on concentration H_2O_2. B2; Zoom on B1, to improve the visualization of 2wt% H_2O_2 size increase.

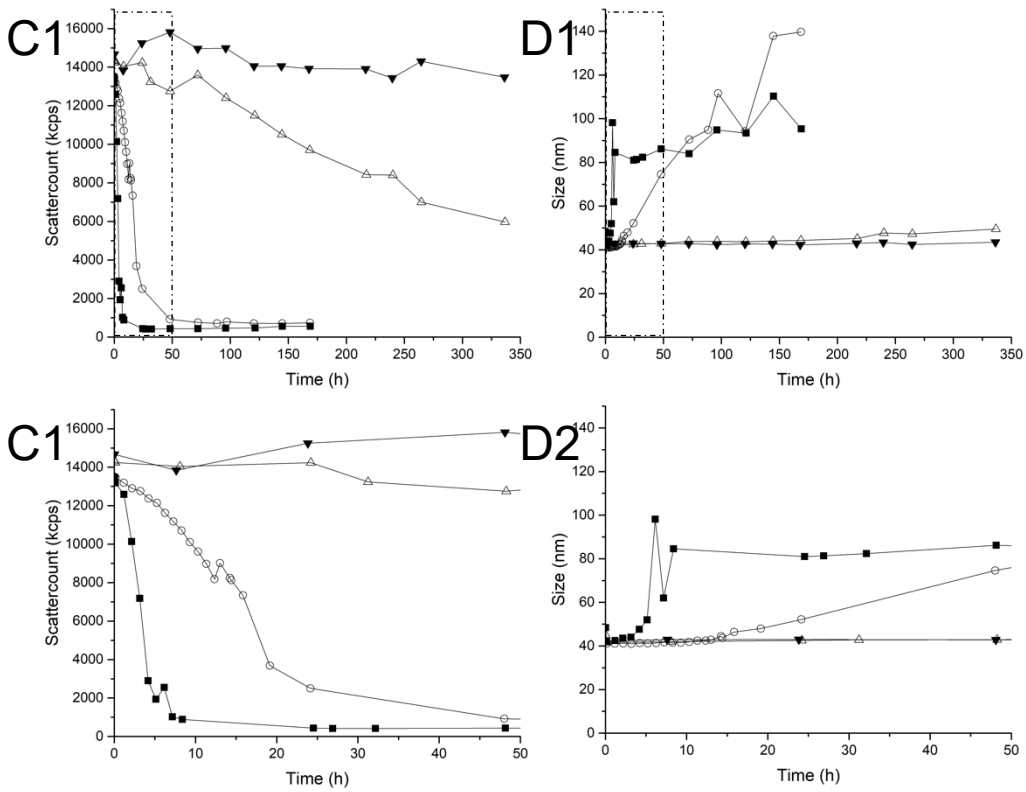

Fig (4.7) (■=2 wt% H_2O_2; ○=0.2 wt% H_2O_2; △=0.007 wt% H_2O_2; ▼= Control (0 wt% H_2O_2) C1; Normalized light intensity scattering for $PD_{85}M_{26}$ after 2 or 0.2 wt% H_2O_2 addition, light intensity scattering decreases to a fixed minimum, 0.007wt% H_2O_2 addition compared with control decreases significantly over time. C2; Zoom on C1 to improve visualization of 2wt% H_2O_2 decrease in light intensity scattering D1; Z-average after H_2O_2 addition for $PD_{85}M_{26}$, initial size is around 40 up to 50 nm and goes up for 2 wt% and 0.2 wt% to 100-140 nm 0.007 wt% H_2O_2 additions was too little to fully convert the Z-average change. D2; Zoom on D1, to improve the visualization of the Z-average increase by 2 wt% H_2O_2.

To visualize PD_XM_Y micelles morphological change after addition of H_2O_2, micellar solutions were exposed to 2 wt% H_2O_2 and observed by stained TEM. After addition of 2 wt% H_2O_2 the number of particles significantly drops within 48 hours (Fig 4.8). The stain is used to visualize the micelles and the stain is attached to the outer shell. After addition of H_2O_2 the micelles should decompose and the stain should be dispersed homogenously. After addition of 2 wt% H_2O_2, the micelles completely decompose, and none of the original structures are observed. Concluding that H_2O_2 addition leads to decomposition of the micelles.

To visualize PD_XM_Y micelles morphological change after addition of 0.2 wt% H_2O_2, (without changing the micelles environment) micelles are observed after addition of H_2O_2 by Cryo-EM. After addition of 0.2 wt% of H_2O_2 the number of particles gradually goes down for PD_XM_Y, few big particles are observed with $PD_{130}M_{16}$ 27hours after H_2O_2 addition (Fig 4.9 C). Thus, the 2 wt% and 0.2 wt% additions of H_2O_2 makes micelles change in morphology, for the $PD_{85}M_{26}$ it leads to complete decomposition of the particles (Fig 4.9 F). The increase in scattering count after addition of H_2O_2 observed by DLS for the $PD_{130}M_{16}$ micelles (Fig 4.7 A), can be caused by the formation of few bigger particles with sizes in order of 10^2 nm (Fig 4.9 C). However, it should be noted that, no conclusions can be made on what is not seen on a TEM, for example on Fig 4.8 B. However, DLS data is in line with all TEM pictures and thus it gives a strong indication that the observations by TEM or Cryo-EM are true, including for example Fig 4.8 B. Concluding that addition of H_2O_2 leads to complete decomposition for $PD_{85}M_{26}$ and almost full decomposition of $PD_{130}M_{16}$ with formation of few enlarged particles.

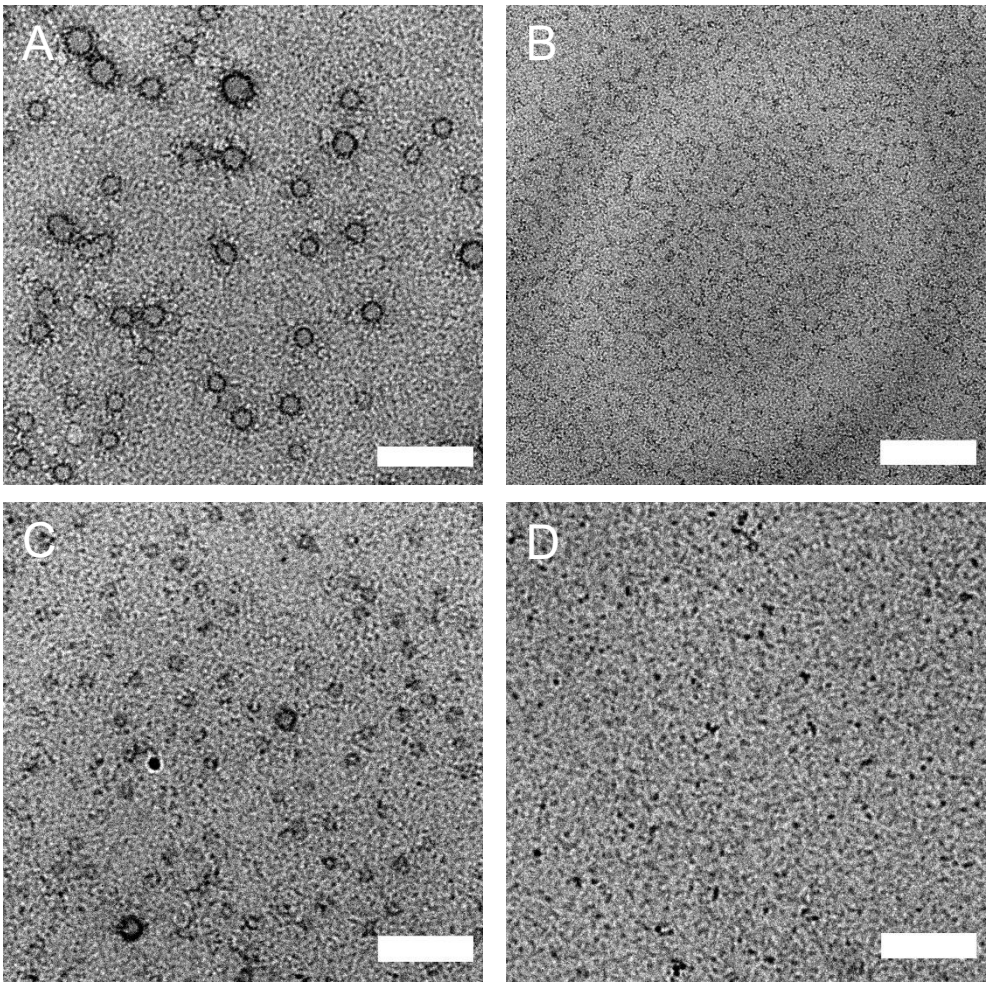

Fig (4.8) Scalebar=100nm A; Stained TEM of $PD_{85}M_{26}$ micelles before addition of 2 wt% H_2O_2. B; Stained TEM $PD_{85}M_{26}$ micelles with 2 wt% H_2O_2 addition after 24 up to 48 hours. C; Stained TEM of $PD_{130}M_{16}$ micelles before addition of 2 wt% H_2O_2. D; Stained TEM $PD_{130}M_{16}$ with 2 wt% H_2O_2 addition after 24 up to 48 hours.

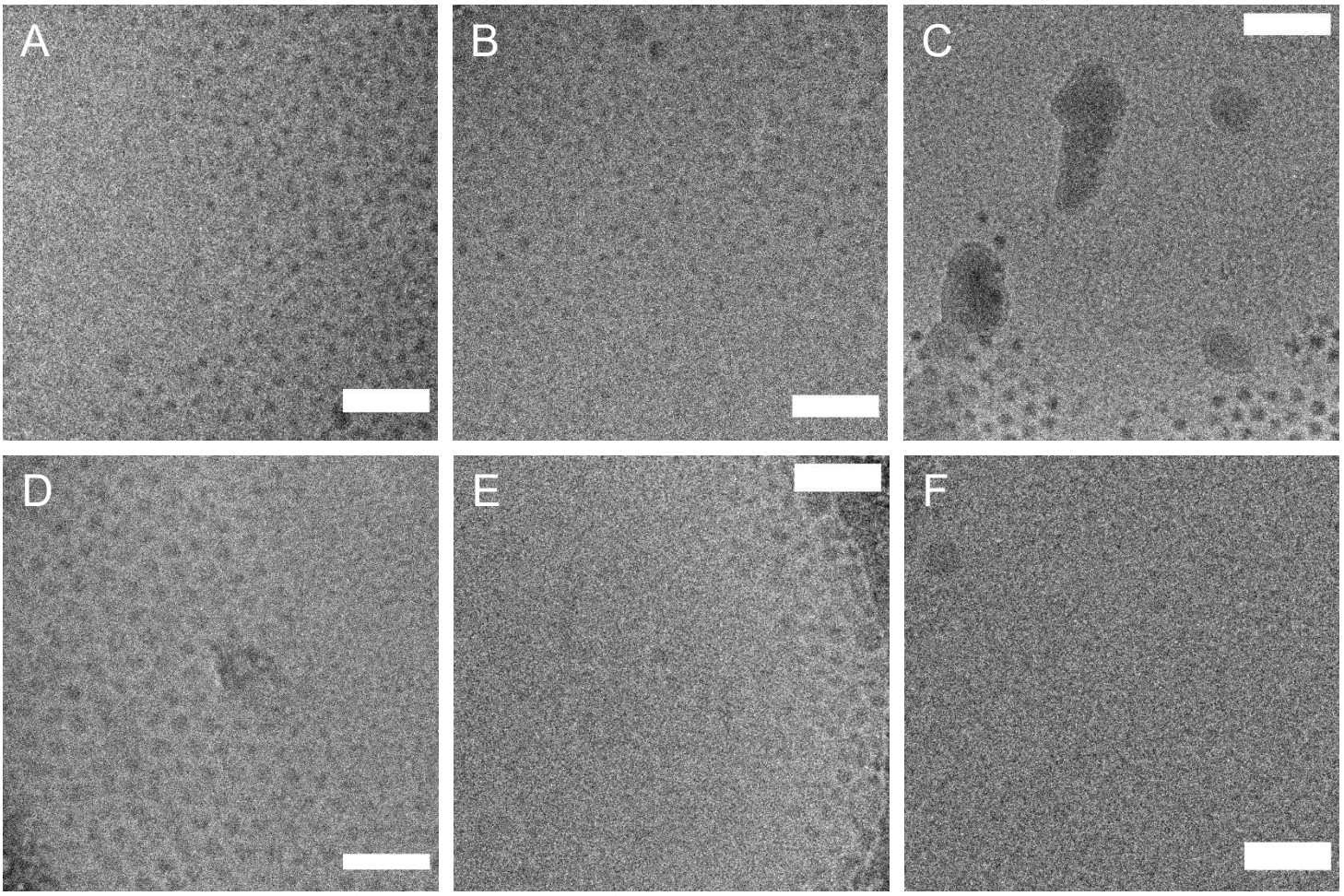

Fig (4.9) Scalebar=100nm A; Cryo-EM of $PD_{130}M_{16}$ ~10mg/ml in PB before 0.2 wt% H_2O_2 addition, small spherical monodisperse micelles are observed. B; Cryo-EM of $PD_{130}M_{16}$ ~10mg/ml in PB 14 hours after 0.2 wt% H_2O_2 addition, less micelles are seen and a few bigger particles are observed. C; Cryo-EM of $PD_{130}M_{16}$ ~10mg/ml in PB 27 hours after 0.2 wt% H_2O_2 addition, still a few micelles are seen but also several big particles are observed. D; Cryo-EM of $PD_{85}M_{26}$ ~10mg/ml in PB before 0.2 wt% H_2O_2 addition, small spherical monodisperse micelles are seen. E; Cryo-EM of $PD_{85}M_{26}$ ~10mg/ml in PB 27 hours after 0.2 wt% H_2O_2 addition, very few particles are still seen. F; Cryo-EM $PD_{85}M_{26}$ ~10mg/ml in PB 43 hours after 0.2 wt% H_2O_2 addition, only one particle is observed which is bigger than the initial micelles.

Micelles drug loading and drug release (determined by fluorescence measurements)

To demonstrate that PD_XM_Y micelles can be loaded with nonpolar model drugs, NR is used. After formation of micelles with the *general procedure PB*, NR was added and incubated. The model drug loading was measured by isolating the micelles from its environment and dissolving it in DMF. 3µg/ml was loaded in the $PD_{85}M_{26}$ micelles and 2µg/ml was loaded in the $PD_{130}M_{16}$ micelles. The small amount of NR-loading could be explained by an inaccurate procedure, during the isolating steps described in the experimental, the extraction of surrounding PB of the micelles always limits the yield by coextracting also model drug loaded micelles. Because the extraction is performed 4 times; this can majorly influence the total drug loading. In literature micellular systems are even drug loaded up to concentrations of mg/g of polymer, which is a factor 1000 difference.[59] Thus, the previous described NR-loading numbers, can only be used for comparison with each other, but cannot be used as absolute numbers.

To demonstrate H_2O_2 triggered drug release of PD_XM_Y micelles, NR loaded micelles are exposed to different concentrations of H_2O_2. NR is fluorescent in a hydrophobic environment such as within PD_XM_Y micelles, and it is not fluorescent in PB. Thus, if the fluorescence intensity decreases, NR is released from the micelles. A decrease in fluorescence is observed when micelles are exposed to 2 wt% and 0.2 wt% H_2O_2 (Fig 4.10). $PD_{85}M_{26}$ takes 5 hours at 37°C until all emission was quenched whilst $PD_{130}M_{16}$ only takes 3 hours at 37°C until all emission was quenched, (these results are presented in a similar way as in reference[50]). The difference in time, could be explained by the difference in chain length of the MTPA block. Next, with 0.007 wt% H_2O_2 addition, change in fluorescence is observed, over a longer period (SI 4.6). However, the control (0 wt% H_2O_2 addition) decreased equally quick as the 0.007 wt% H_2O_2 addition, concluding that the 0.007 wt% H_2O_2 addition did not give a significant difference in the NR release rate, so no conclusions can be made from this experiment. Furthermore, from the control experiments we can conclude that the NR emission over time is quenched. This can be caused by: that NR is leaking, that NR is aggregating or that the NR is degrading. Lastly, the amount of emission at t=0 is for the $PD_{85}M_{26}$ higher (compared to $PD_{130}M_{16}$), confirming that $PD_{85}M_{26}$ has a higher model drug loading compared to $PD_{130}M_{16}$. To conclude, micelles release NR at the same rate as the micelles decompose shown in previous DLS data (Fig 4.7). Meaning that the NR release is caused by micelles decomposition triggered by H_2O_2 addition, for the 2 wt% and 0.2 wt% H_2O_2 addition. However, due to very similar behavior between control and 0.007 wt% no conclusions can be made, about the sensitivity of drug release. Overall, NR is a suitable model drug for drug release experiments if the measurements do not exceed 24 hours and high drug loading is not relevant.

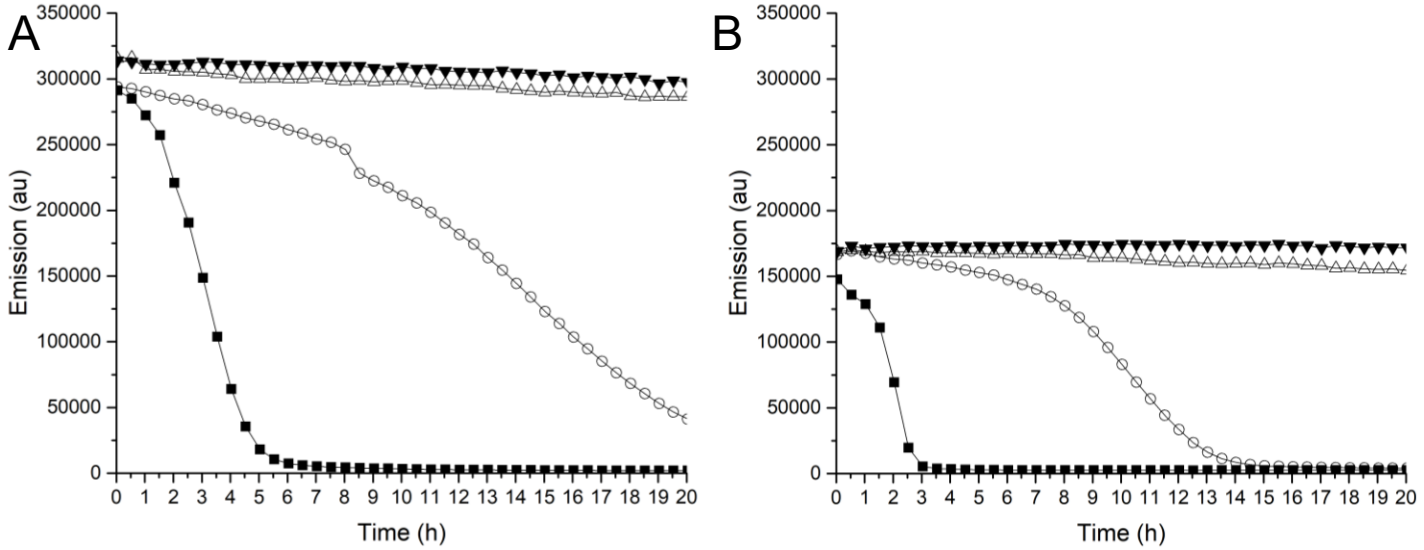

Fig (4.10) (■=2 wt% H_2O_2; ○= 0.2 wt% H_2O_2; △ =0.007 wt% H_2O_2; ▼= Control (0 wt% H_2O_2)) Emission of NRs maximum measured at 633nm with autosampler over time at 37°C A; Emission of Nile reds maximum over time in $PD_{85}M_{26}$ micelles in PB after H_2O_2 addition, emission fully quenched within 5 hours after 2 wt% H_2O_2 addition. NOTE at emission around 250,000 au a drop in emission is detected this is better visible in SI (4.6) this is probably caused by a change in the slit by the device. B; Emission of NRs maximum in $PD_{130}M_{16}$ micelles in PB solution, emission fully quenched within 3 hours after 2 wt% H_2O_2 addition.

In way to perform release experiments, for longer than 24 h and to use a real drug for eventual cells experiments, we continued using the real drug doxorubicin (DOX) for release experiments. The experiment is executed by putting loaded DOX/$PD_{130}M_{16}$ micelles in a dialysis bag with pore size of 14 kDa and the solvent around the dialysis bag is measured by fluorescence at 37 °C over time (Fig 4.11 A). DOX is fluorescent within the micelles as well as outside micelles, however, literature does mention that DOX fluorescence behaves differently per environment.[55] The fluorescent DOX is found immediately after addition of H_2O_2, however, also without the addition of H_2O_2, DOX is detected. Even though, the release with H_2O_2 was slightly quicker not a relevant difference was observed compared to the 0 wt% H_2O_2. After 8 hours the signal of the sample with 2 wt% H_2O_2 decreased rapidly whilst the one with 0 wt% H_2O_2 kept increasing. Beside a control with 0 wt% H_2O_2, a control without polymer is performed, with and without H_2O_2 addition (Fig 4.11 B). Concluding that the DOX in combination with 2 wt% H_2O_2 degrades. To investigate the increase of the 0 wt% H_2O_2 fluorescence after dilution in water (Fig 4.11A). DOX was detected by measuring the fluorescence signal after diluting (Fig 4.11 B). Normally diluting decreases the amount of fluorescence however, at very high concentration DOX fluorescence will quench and become less fluorescent. Thus, diluting the DOX results in increased fluorescence. To verify that DOX degrades by H_2O_2 addition and not by elevated temperature or by interaction with the dialysis bag, DOX was exposed to a diluted environment with 2 wt% H_2O_2. Diluting DOX resulted, thus indeed, in an increase of fluorescence. 2 wt% H_2O_2 addition led again to decrease in fluorescence implicating that degradation occurred. In conclusion, it is indistinct if the micelles have encapsulated DOX and it is unclear if the increase in temperature had influence in drug release or degradation. Furthermore, it seems that DOX is not properly diffused outside the dialysis bag, affecting the fluorescence intensity of the sample taken in the medium around it.

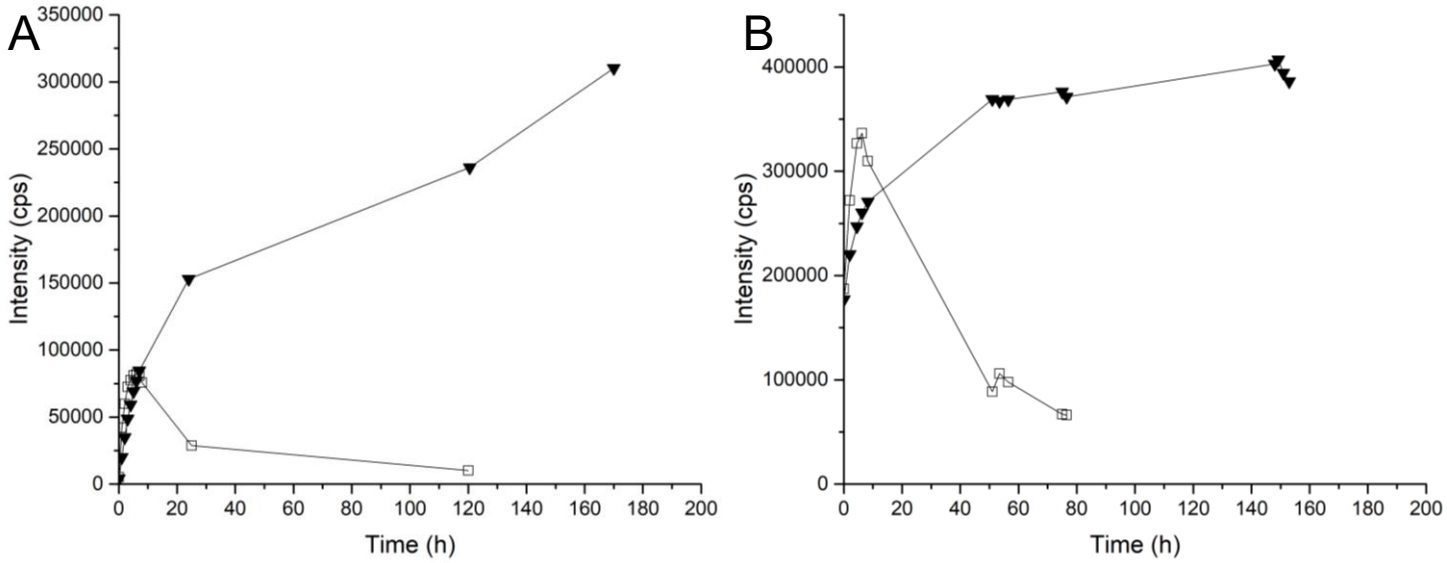

Fig (4.11) (▼=Control (0 wt% H_2O_2), □=2 wt% H_2O_2) Emission maximum of DOX at 500nm over time A; $PD_{130}M_{16}$ with DOX after addition of 2 wt% H_2O_2 by investigating the surroundings of the dialysis bag at 37°C, a sudden increase in fluorescence was observed around dialysis bag indicating release of DOX from the inside. However, control has similar release speed and continues. B; DOX without $P_{130}M_{16}$ and without dialysis bag at R.T. after addition of 2 wt% H_2O_2. Show similar trends as in Fig 4.11 A (initial value higher by not using dialysis bag but total volume). Increase of control can be explained by formation of aggregates that decompose after dilution which would increases fluorescence.

To prevent degradation due to increase in temperature and the interaction with dialysis bag a similar experiment was done, by combining the experiments performed for Fig 4.11 A and B. This was done to investigate whether PD_XM_Y micelles encapsulate DOX. As visible in Fig 4.11 B the control settles at around 96 hours. During this experiment, at 96 hours after diluting, H_2O_2 was added to observe what influence it has on the DOX fluorescence with and without micelles (SI 4.7). Without micelles, the signal drops directly, H_2O_2 reacts with DOX, and quenching the fluorescence (Fig 4.12 B). With micelles the signal initially increases, meaning that more DOX becomes fluorescent, this gives a strong indication that H_2O_2 helped releasing aggregated DOX from the micelles which can dissolve and become fluorescent by the increase of total volume (Fig 4.12A). With 2 wt% the same phenomenon is observed as in Fig 4.11 A, namely that after 8 hours the degradation is dominant over the increase in fluorescence, meaning that DOX degrades. For the sample with 0.2 wt% H_2O_2 addition the fluorescence becomes even higher, this gives an indication that the lower concentration H_2O_2 influences the degradation less giving DOX more time to dissolve and become more fluorescent before it degrades. For 0.007 wt% this

statement is confirmed, SI (4.8). For the control (0 wt% H_2O_2), it seems very stable with a slight decrease in several weeks' time. The initial rise in fluorescence after diluting, must be caused by the dissolved aggregates DOX and maybe partly by DOX that was weakly bound to the micelles. It can be concluded that micelles do encapsulate DOX, with relatively large amounts, and that the DOX even aggregates within the micelles. It appears that after H_2O_2 addition DOX is released leading to an increased fluorescence, and simultaneously the H_2O_2 degrades DOX, which leads to an eventual decrease in fluorescence, meaning the exact quantitative amount of encapsulated DOX cannot be calculated. So, the two seemingly proven observations are that $PD_{130}M_{16}$ micelles do encapsulate, highly likeable aggregated, DOX and they are able to release it with different concentrations of H_2O_2 down to 0.007 wt% H_2O_2 addition.

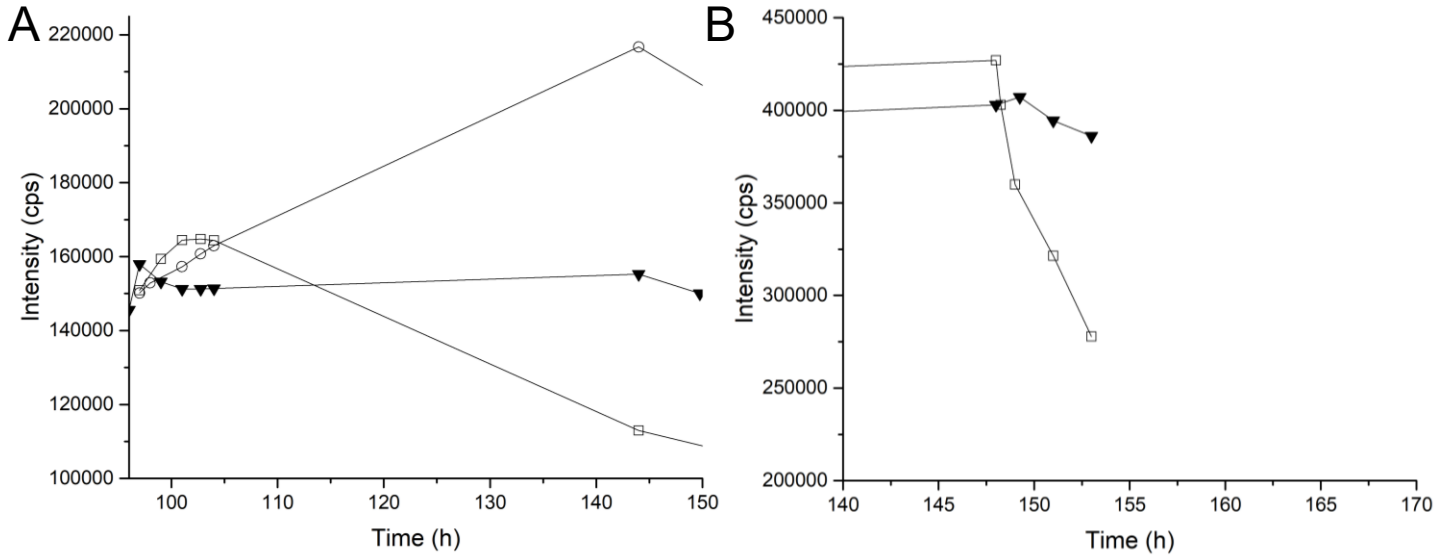

Fig (4.12) Emission of DOXs maximum at 590nm over time (▼= 0 wt% H_2O_2, □ = 2 wt% H_2O_2, ○=0.2 wt% H_2O_2) A; $PD_{130}M_{16}$ with DOX at R.T. after 96 hours after dilution, H_2O_2 was added. Addition of H_2O_2 led to increase in fluorescence by decomposing micelles leading to aggregated DOX in micelles to be dissolved and become more fluorescent. B; DOX without $PD_{130}M_{16}$ at R.T. after 148 hours of dilution H_2O_2 was added. No increase of fluorescence was observed after H_2O_2 addition.

Micelles interaction with external radiation (determined by ^{1}H-NMR, DLS, fluorescence measurements)

To investigate if radiation affects the polymer structure in micelles configuration, PD_XM_Y was irradiated with 500 Gy gamma radiation using the ^{60}Co source. PD_XM_Y micelles in PB were made according to *general procedure PB* and irradiated with 500 Gy, 30 min after radiation a ^{1}H-NMR was made in (10 V%) D_2O/PB mixture. No significant difference was observed compared before and after gamma radiation, which were not detected (Fig 4.13). ^{1}H-NMR is not extremely sensitive, so it is possible that some micelles did collapse due to gamma radiation. At chemical shift 2.8 up to 3.1ppm is the DMA region, after radiation this seems to become a weaker signal compared to the control. Normalizing the ^{1}H-NMR by the D_2O peak is inaccurate, so previous observation can be misleading. Concluding that micelles behave different after radiation compared to H_2O_2 addition (Fig 4.6), which was not expected. Furthermore, no chemical reaction is observed.

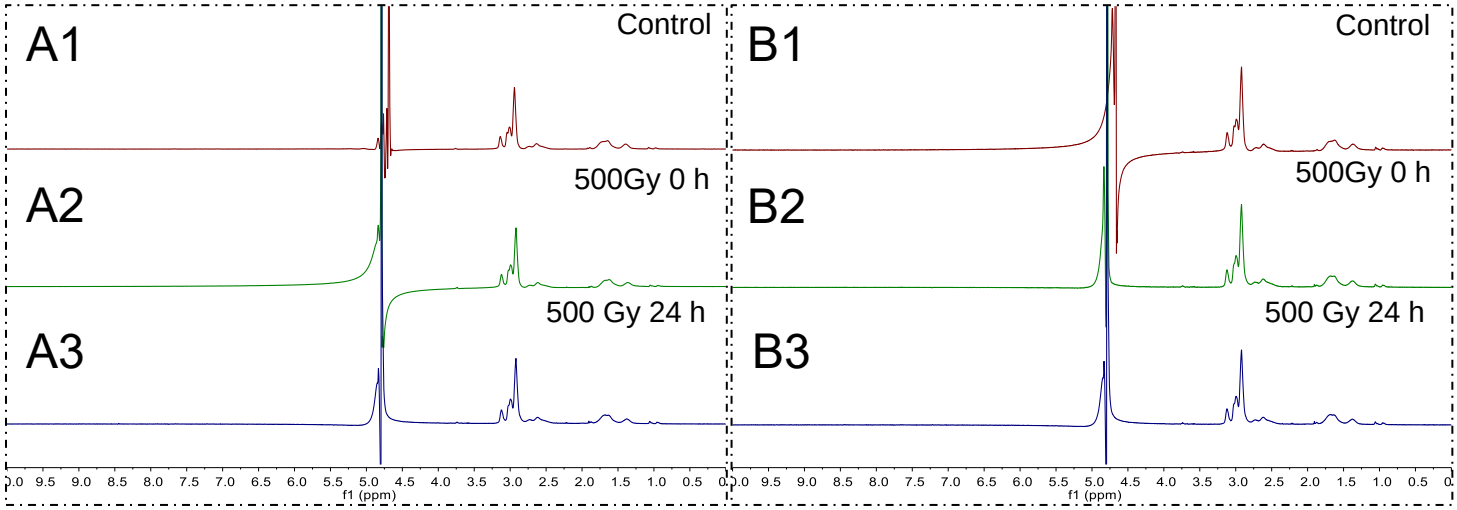

Fig (4.13) ^{1}*H-NMR (400 MHz, D_2O);* A; A1, ^{1}H-NMR of $PD_{130}M_{16}$ before 500 Gy radiation; A2, ^{1}H-NMR of $PD_{130}M_{16}$ directly after 500 Gy radiation; A3, ^{1}H-NMR of $PD_{130}M_{16}$ 24 hours after 500 Gy radiation. B; ^{1}H-NMR of $PD_{85}M_{26}$ before 500 Gy radiation; A2, ^{1}H-NMR of $PD_{85}M_{26}$ directly after 500 Gy radiation; A3, ^{1}H-NMR of $PD_{85}M_{26}$ 24 hours after 500 Gy radiation.

To verify that radiation did not disrupt the polymer ($PD_{130}M_{16}$) in micelles configuration, GPC with THF was used. GPC would show a longer retention time in a size exclusion column if the polymer would become smaller after radiation. The GPC measurement showed before and after radiation a wide peak, a difference is observed between the two samples where the radiated sample led to a small extra peak SI (4.8). There are 2 reasons why GPC is not suited to draw strong conclusions. Firstly, the retention time of the polymer was so wide that the representing polymer peak exceeded partly the time of 11 minutes, which would be the equivalent time the solvent would need to flow through. This, probably is caused by interaction of the polymer with the column, increasing its retention time. Secondly, the GPC coupled to UV at ~254 nm and refractive index measurement gave two signals. But the refractive index signal should be the most accurate, however, the intensity of the signal is relatively weak. Overall concluding that radiation did affect the polymer somewhat, but no further conclusions can be made.

To investigate the morphological change of PD_XM_Y micelles after radiation, micelles were prepared in PB according to *general procedure PB* and exposed to different doses between 0 and 500 Gy of gamma radiation. After radiation, the solution was measured over time by DLS. The light intensity plot of $PD_{130}M_{16}$, with doses of 120 and 500 Gy, gave a clear difference in size distribution caused by radiation. And a direct increase in hydrodynamic diameter and increase in light intensity scattering was observed (Fig 4.14). $PD_{85}M_{26}$ micelles with a dose of 67 Gy show no difference, comparing Fig 4.14 A2 with SI 4.9. Previous experiments show that after H_2O_2 addition a decrease in light intensity scattering is observed. But after irradiation with doses of 120 and 500 Gy, the light intensity scattering increases meaning that micelles do not degrade due to gamma radiation but seem to break and cluster leading to an increase in size and thus, also an increase in light intensity scattering. Furthermore, the light intensity scattering goes down in time, indicating that the new formed structures reorientate to structures with similar size as the original micelle, indicating that the change caused by gamma radiation is only temporarily. It can therefore be concluded that after exposure to external gamma radiation micelles behave differently compared to H_2O_2 addition, furthermore the increase in size is explained by micelles and part of micelles which cluster.

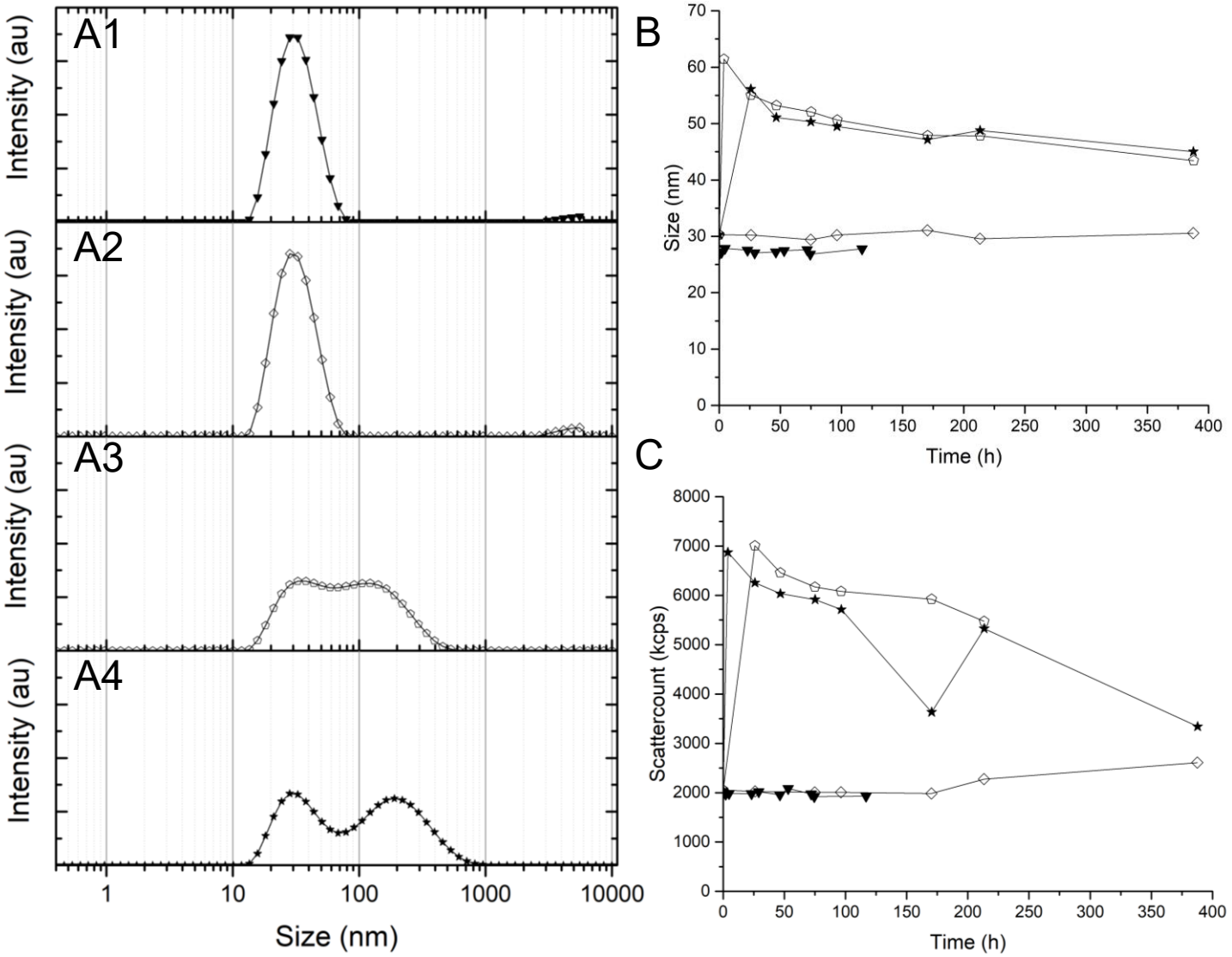

Fig (4.14) (▼= control (0 Gy), ◇= 67 Gy, ⬠= 120 Gy, ★=500Gy) At t=0 the sample was not radiated and after radiation the sample was measured within hours and traced over time. A; Light intensity plots of $PD_{130}M_{16}$ micelles at different radiation dose in PB. B; Z-average over time of $PD_{130}M_{16}$ after radiation, the z-average becomes smaller days after radiation. C; Scattering count of $PD_{130}M_{16}$ after radiation, scattering count initially increases and over time almost meets the control again.

To verify that the change in size is indeed not due to formation of H_2O_2 by radiolysis which should decompose the micelles, but by a different effect caused by the external radiation, the radical scavenger HEPES (100mM, pH 7.4) is used.[60] $PD_{130}M_{16}$ micelles were made in HEPES and exposed to different dose between 0 and 500 Gy and observed by DLS (Fig 4.15 A). Visible in the light intensity plot is that even 82 Gy caused a difference in the size distribution. This effect is thus caused without ROS such as H_2O_2 because, radicals should be scavenged by the HEPES buffer. Change in hydrodynamic diameter and scattering count is observed, giving again a strong indication that the micelles cluster. DLS is calibrated with HEPES for RI and viscosity parameters, thus the difference in initial size compared to PB is due to the difference in solvent, and not due to wrong parameter input. No over time control measurement was performed for micelles in HEPES, and over time stability is thus assumed. Compared to $PD_{130}M_{16}$ micelles in PB the initial size is around 42 nm instead of 30 nm and thus initial light intensity scattering is also higher from 2,000 kcps up to 2,500 kcps (Fig 4.1 & Fig 4.15 B). Indicating that bigger micelles are formed in HEPES, and these micelles are also sensitive to 82 Gy of gamma irradiation. For $PD_{85}M_{26}$ see SI (4.10) no significant difference is observed after radiation in light intensity distribution, a slight increase in hydrodynamic size and light intensity scattering, but not a comparable change as with $PD_{130}M_{16}$. Meaning that $PD_{85}M_{26}$ is more resistant to gamma radiation, than $PD_{130}M_{16}$. Concluding that $PD_{130}M_{16}$ micelles are sensitive to gamma radiation but behave differently as with H_2O_2 addition. $PD_{85}M_{26}$ is not sensitive to gamma radiation. HEPES buffer increases the initial micelles hydrodynamic diameter, and the $PD_{130}M_{16}$ micelles tend to cluster after gamma radiation, even though the formed ROS are scavenged by HEPES.

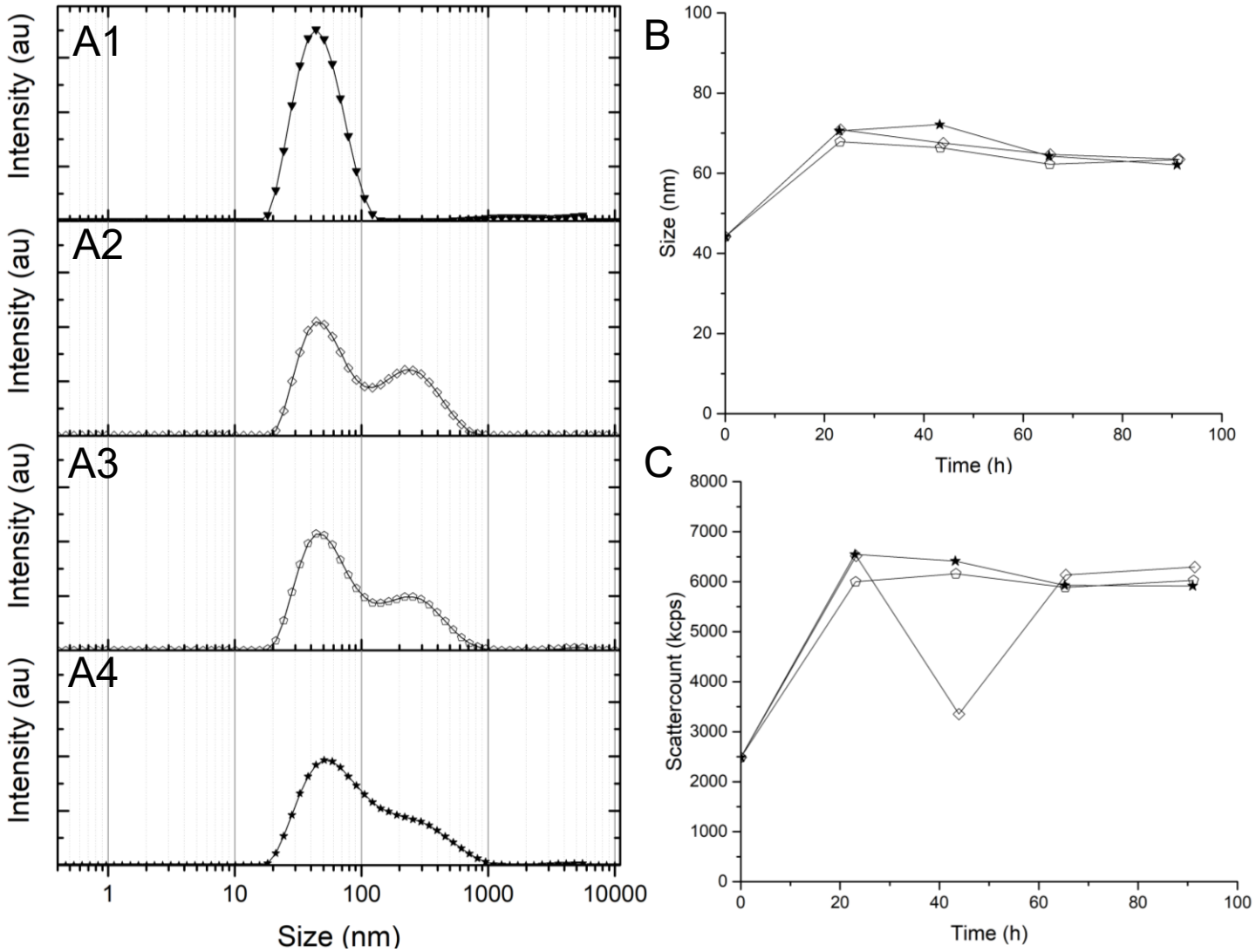

Fig (4.15) (▼=0 Gy, ◇=82 Gy, ⬠=120 Gy, ★=500 Gy) At t=0 the samples were not irradiated, 18 hours after initial measurement, the samples got irradiated and tracked by DLS within hours. A; Light intensity plots $PD_{130}M_{16}$ micelles in HEPES after different radiation dose. B; Z-average over time after different dose of radiation. C; Light intensity scattering over time after different dose of radiation.

To investigate the effect of gamma radiation on the drug release, $PD_{130}M_{16}$ micelles with DOX in PB were made. 96 hours after dilution, the samples got irradiated with different dose (SI 4.11), fluorescence intensity was measured over time. After radiation, a rapid decrease in fluorescence is observed which could indicate that DOX is degraded, however, in time the fluorescence intensity increases (Fig 4.16A). Because the signal increases, DOX cannot be completely degraded, the fluorescence is temporarily quenched by aggregating micelles which hinder excitation and emission. The control, where no $PD_{130}M_{16}$ was added, shows similar behavior. This gives an indication that DOX also clusters in solution and becomes less fluorescent without micelles (Fig 4.16B). The amount of initial emission before radiation is not observed anymore, indicating that some DOX is permanently degraded due to the gamma radiation, meaning that gamma radiation quenches DOX fluorescence. Furthermore, the clustering of micelles can prevent excitation of DOX contributing to the decrease of emission. It can therefore be concluded that gamma radiation clusters DOX and micelles resulting in quenching fluorescence intensity.

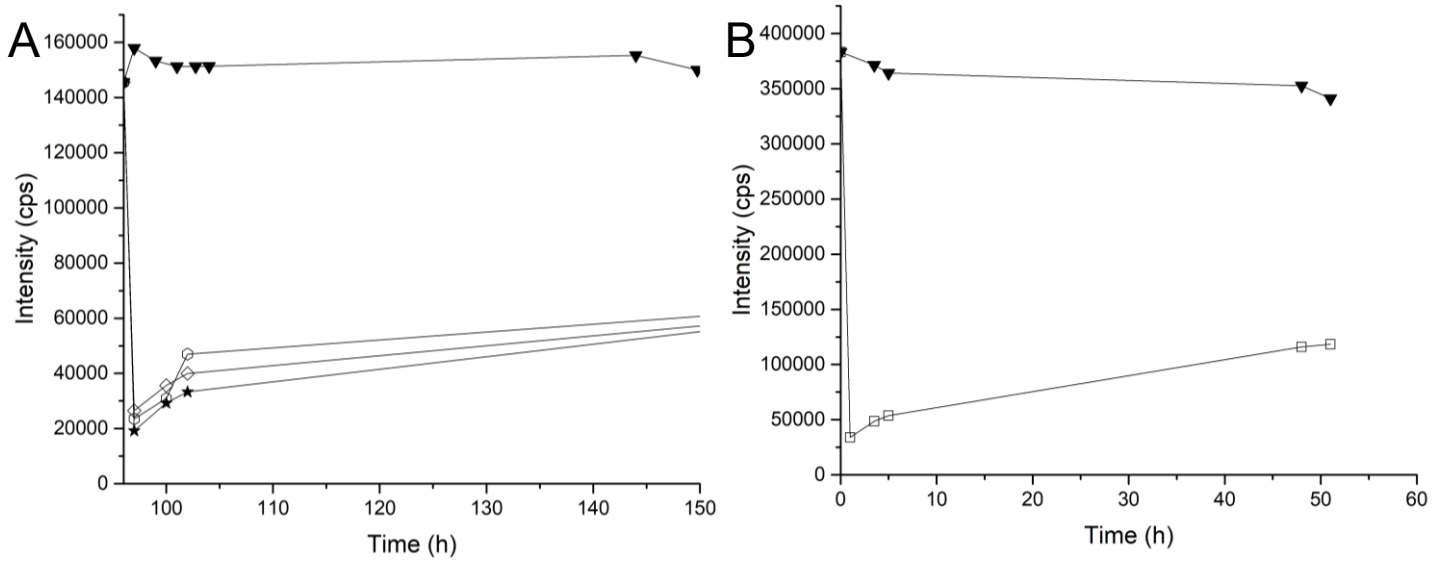

Fig (4.16) Emission of DOXs maximum at 590nm over time. At t=0 the sample was not radiated and after radiation the sample was measured within hours. A; (▼=0 Gy, ◇= 60Gy, ⬡= 120 Gy, ★= 500 Gy) $PD_{130}M_{16}$ with DOX at R.T. 96 hours after dilution, samples got exposed to external radiation. External radiation led to a decrease in fluorescence by probably clustering micelles quenching fluorescence of DOX. B; ((▼=0 Gy, □ = 500 Gy) DOX without $PD_{130}M_{16}$ at R.T. after more than 180 hours of dilution sample got radiation with 500 Gy. Immediate decrease in fluorescence, which slowly increases over time.

Micelles radiolabeling (activity measuring)

Lastly, to follow micelles in vivo for drug release purposes, radiolabeling can be used to track micelles with SPECT imaging. By addition of Indium111 in HCl (pH 2) to micelles ($PD_{85}M_{26}$) made in HEPES buffer, the Indium diffused inside the micelles. A radiolabeling efficiency of 12 % was acquired without optimization, such as increasing the micelles concentration. To further investigate if these micelles are suitable for radiolabeling, stability test should be done.

Conclusion

The main goal of this thesis was to establish a drug delivery system based on PD_XM_Y micelles which are sensitive to ROS. This goal was subdivided within three steps previous shown in Fig 2.4. The initial step was to form micelles in water, by addition of PD_XM_Y block copolymer in aqueous condition, DLS and TEM measurement show that micelles were made. The second step was to investigate the interaction of these micelles with ROS. By H_2O_2 addition, down to a concentration of 2mM (SI 4.12), to micellar solutions, decomposition of the micelles was observed by ^{1}H-NMR, DLS and TEM. Afterwards, several attempts to make sufficient ROS by gamma radiation to also decompose PD_XM_Y micelles were made. However, decomposition of micelles was not observed by DLS. The DLS measurements gave a strong indication that micelles after gamma radiation cleaved and clustered micelles, forming bigger particles. Lastly, micelles were (model) drug loaded, by NR addition to the PD_XM_Y micellar solution, even though, quantification of the drug loading failed, drug releases measurements by fluorescence were performed. The pace wherein NR got released was similar to the speed wherein micelles decompose with H_2O_2 addition. When performing similar experiment with DOX instead of NR, the DOX decomposed due to the addition of H_2O_2. This made visualization of drug release with DOX challenging.

This research contributes to the research area, that PD_XM_Y micelles are sensitive to relative low concentrations of ROS, the decomposition mechanism of the PD_XM_Y block copolymer is favorable for controlling drug release speeds. Furthermore, it adds that ROS induced by gamma radiation is not straight forward and can lead to side effects where instead of decomposition of micelles, clustering of micelles can occur. To conclude, PD_XM_Y micelles show promising features to eventually become a suitable drug delivery system, which is sensitive to elevated levels of ROS. However, more research towards cell experiments should be done, to empower the previous statement.

Recommendations

Quantify the (model) drug loading

During this thesis, NR did not perform as expected, but this can maybe be improved. To verify the drug loading of NR within micelles: liquid-liquid extraction could be performed, centrifugal filters (10 kDa) could be used, or a size exclusion column could be used for separation of NR. Still, the problem of NR degradation, within days, would stay a problem. A more stable (model) drug should be considered.

Furthermore, DOX loading in micelles was not able to be quantified. A final recommendation to make DOX more suitable for drug release systems, could be, by tweaking the DOX to polymer ratio. With less DOX addition, oversaturation of the dialysis bag will be prevented. Also, with less DOX addition, it is less likely that DOX aggregates will be formed. To prevent yield loss by the dialysis bag, a column can be used. Instead of separating with dialysis bags, one can use a size exclusion column for drug loading. Beside a column, also liquid-liquid extraction for DOX and micelles can be used. With one of these 2 methods the drug loading of a real drug can be determined more accurate.

Drug release

DOX made hydrophobic should favor drug loading within water. However, during this thesis it was shown that due to the making of hydrophobic DOX, DOX became more reactive to H_2O_2, making the fluorescent property of DOX quench. A more resistant drug should be used or lower concentrations of H_2O_2. Beside hydrophobic DOX also, DOX•HCl can be used which is still fluorescent but will have a lower drug loading.

Increasing the concentration of micelles from 1 mg/ml to 3 mg/ml, will favor every measurement, and Cryo-EM showed that up to 10mg/ml still consist only micelles. Furthermore, it will favor the drug loading capacity and detectability, making it more consistent with the NMR results, which also required increased concentration micelles. It should be noted that with too high concentration of micelles the solution will become turbid making some measurement less reliable.

In depth research of gamma radiation with micelles

Initially was expected that gamma radiation would lead to increased ROS concentration. The increased ROS concentration would induce decomposition of the micelles, likewise as with the H_2O_2 addition experiments.

However, the exact opposite happened. Increased light intensity scattering and decreased fluorescence was observed, this gave a strong indication that micelles aggregated. By increasing the concentration, prior to radiation, Cryo-EM can show if it did aggregate after radiation. The minimal dose for causing a change, observed by DLS, was around 60 Gy. Such dose is equal to the complete dose of an entire treatment, thus way to high. Usage of a catalyst making the micelles more sensitive to gamma radiation is required, for gamma sensitive decomposition of the micelles.

Vesicles

Beside micelles, PD_XM_Y block copolymer could be used to make different nanoparticles such as vesicles. Vesicles have a lower drug loading, however, can, with a suitable procedure, loading polar and nonpolar particles. By changing the ratio between the DMA and MTPA blocks, different nanoparticles should be created. Making this block copolymer versatile.

End group modification

By end group modification the micelles could become an active targeting drug delivery system instead of passive targeting drug delivery system, becoming not solely reliant on blood flow but also on overexpression of tumor specific exterior or interior. The end group, described by L. Reinalda, is very suitable for end group modification, by adjusting several end groups, PD_XM_Y micelles could become suitable for active targeting.

Bibliography

1. Siegel, R. L., Miller, K. D. & Jemal, A. Cancer statistics, 2016. *CA. Cancer J. Clin.* **66**, 7–30 (2016).
2. Siegel, R. *et al.* Cancer treatment and survivorship statistics, 2012. *CA. Cancer J. Clin.* **62**, 220–241 (2012).
3. Gupta, R. & Rai, B. *Computer-Aided Design of Nanoparticles for Transdermal Drug Delivery*. *Methods in Molecular Biology* **2059**, (2020).
4. Zhang, P. *et al.* A Multistage Cooperative Nanoplatform Enables Intracellular Co-Delivery of Proteins and Chemotherapeutics for Cancer Therapy. *Adv. Mater.* **2000013**, 1–11 (2020).
5. Paganelli, G. & De Santis, R. Antibody-based cancer therapies: Back to 'polyclonals'? *Eur. J. Nucl. Med. Mol. Imaging* **31**, 1453–1455 (2004).
6. Cimadamore, A. *et al.* New prostate cancer targets for diagnosis, imaging, and therapy: Focus on prostate-specific membrane antigen. *Front. Oncol.* **8**, 1–11 (2018).
7. Geou-Yarh Liou, P. S. Reactive oxygen species in cancer. **44**, (2010).
8. Wu, Y. *et al.* Co-delivery of dual chemo-drugs with precisely controlled, high drug loading polymeric micelles for synergistic anti-cancer therapy. *Biomater. Sci.* **8**, 949–959 (2020).
9. Lv, S. *et al.* High Drug Loading and Sub-Quantitative Loading Efficiency of Polymeric Micelles Driven by Donor-Receptor Coordination Interactions. *J. Am. Chem. Soc.* **140**, 1235–1238 (2018).
10. Zhao, Y. Z. *et al.* Characterization and anti-tumor activity of chemical conjugation of doxorubicin in polymeric micelles (DOX-P) in vitro. *Cancer Lett.* **311**, 187–194 (2011).
11. Yoo, H. S. & Park, T. G. Biodegradable polymeric micelles composed of doxorubicin conjugated PLGA-PEG block copolymer. *J. Control. Release* **70**, 63–70 (2001).
12. Mohan, P. & Rapoport, N. Doxorubicin as a Molecular Nanotheranostic Agent.pdf. **7**, 1959–1973 (2010).
13. Gong, J., Chen, M., Zheng, Y., Wang, S. & Wang, Y. Polymeric micelles drug delivery system in oncology. *J. Control. Release* **159**, 312–323 (2012).
14. Fantel, A. G. Reactive oxygen species in developmental toxicity: Review and hypothesis. *Teratology* **53**, 196–217 (1996).
15. Gupta, S. C. *et al.* Upsides and downsides of reactive oxygen species for Cancer: The roles of reactive oxygen species in tumorigenesis, prevention, and therapy. *Antioxidants Redox Signal.* **16**, 1295–1322 (2012).
16. Han, D., Williams, E. & Cadenas, E. Mitochondrial respiratory chain-dependent generation of superoxide anion and its release into the intermembrane space. *Biochem. J.* **353**, 411–416 (2001).
17. Nosaka, Y. & Nosaka, A. Y. Generation and Detection of Reactive Oxygen Species in Photocatalysis. *Chem. Rev.* **117**, 11302–11336 (2017).
18. Pardridge, W. M. Molecular Trojan horses for blood-brain barrier drug delivery. *Curr. Opin. Pharmacol.* **6**, 494–500 (2006).
19. Xue, X. *et al.* Trojan Horse nanotheranostics with dual transformability and multifunctionality for highly effective cancer treatment. *Nat. Commun.* **9**, (2018).
20. Soh, N. Recent advances in fluorescent probes for the detection of reactive oxygen species. *Anal. Bioanal. Chem.* **386**, 532–543 (2006).
21. Gomes, A., Fernandes, E. & Lima, J. L. F. C. Fluorescence probes used for detection of reactive oxygen species. *J. Biochem. Biophys. Methods* **65**, 45–80 (2005).
22. Sun, Y., Yin, X. F., Ling, Y. Y. & Fang, Z. L. Determination of reactive oxygen species in single human erythrocytes using microfluidic chip electrophoresis. *Anal. Bioanal. Chem.* **382**, 1472–1476 (2005).

23. Mubarakshina, M. M. *et al.* Production and diffusion of chloroplastic H2O2 and its implication to signalling. *J. Exp. Bot.* **61**, 3577–3587 (2010).

24. Raedschelders, K., Ansley, D. M. & Chen, D. D. Y. The cellular and molecular origin of reactive oxygen species generation during myocardial ischemia and reperfusion. *Pharmacol. Ther.* **133**, 230–255 (2012).

25. Rhee, S. G. H2 O2 , a Necessary Evil for. *Science (80-.).* **312**, 1882–1884 (2006).

26. Jackson, M. J. & Mcardle, A. Age-related changes in skeletal muscle reactive oxygen species generation and adaptive responses to reactive oxygen species. *J. Physiol.* **589**, 2139–2145 (2011).

27. Adam-Vizi, V. & Starkov, A. A. Calcium and mitochondrial reactive oxygen species generation: How to read the facts. *J. Alzheimer's Dis.* **20**, (2010).

28. Weinber, R. A. Fundamental Understandings. *Sci. Am.* **275**, 61–61 (1996).

29. Olsen, J. Causes and Prevention. *Scand. J. Public Health* **19**, 1–6 (1991).

30. Jensen, M. B., Ejlertsen, B., Mouridsen, H. T. & Christiansen, P. Improvements in breast cancer survival between 1995 and 2012 in Denmark: The importance of earlier diagnosis and adjuvant treatment. *Acta Oncol. (Madr).* **55**, 24–35 (2016).

31. An, F., Chan, M., Kommidi, H., Ting, R. & Medicine, W. C. Tools for Imaging in Oncology. **207**, 266–273 (2016).

32. Nygren, P. What is cancer chemotherapy? *Acta Oncol. (Madr).* **40**, 166–174 (2001).

33. Tang, J. *et al.* Postmortem oxygen consumption by mitochondria and its effects on myoglobin form and stability. *J. Agric. Food Chem.* **53**, 1223–1230 (2005).

34. Trachootham, D., Alexandre, J. & Huang, P. Targeting cancer cells by ROS-mediated mechanisms: A radical therapeutic approach? *Nat. Rev. Drug Discov.* **8**, 579–591 (2009).

35. Xu, Q., He, C., Xiao, C. & Chen, X. Reactive Oxygen Species (ROS) Responsive Polymers for Biomedical Applications. *Macromol. Biosci.* **16**, 635–646 (2016).

36. Liou, G.-Y. & Storz, P. Reactive oxygen species in cancer. *PMC* **44**, (2014).

37. Joshi, C. *et al.* Practical and clinical considerations in Cobalt-60 tomotherapy. *J. Med. Phys.* **34**, 137–140 (2009).

38. Rice-Evans, P. & Aung, Z. Bemerkung zur Arbeit On the decay of cobalt 60. *Zeitschrift für Phys.* **245**, 386 (1971).

39. Hans-Jurgen Biersack, L. M. F. *Clinical Nuclear Medicine*. *Journal of Chemical Infomation and Modeling* **53**, (2007).

40. Liu, H., Carter, P. J. H., Laan, A. C., Eelkema, R. & Denkova, A. G. Singlet Oxygen Sensor Green is not a Suitable Probe for 1O2 in the Presence of Ionizing Radiation. *Sci. Rep.* **9**, 1–8 (2019).

41. Ltd, M. intestruments. FAQWill Backscatter And 90 Degree Results Be Consistent ? 1–4 Available at: https://www.materials-talks.com/wp-content/uploads/2015/10/backscatter-vs-90.pdf. (Accessed: 9th February 2021)

42. Acharya, R. Interaction of waves with medium. *Satell. Signal Propagation, Impair. Mitig.* 57–86 (2017). doi:10.1016/b978-0-12-809732-8.00003-x

43. Bhattacharjee, S. DLS and zeta potential - What they are and what they are not? *J. Control. Release* **235**, 337–351 (2016).

44. Amin, S., Barnett, G. V., Pathak, J. A., Roberts, C. J. & Sarangapani, P. S. Protein aggregation, particle formation, characterization & rheology. *Curr. Opin. Colloid Interface Sci.* **19**, 438–449 (2014).

45. Alkholidi, A. G. & Altowij, K. S. Free Space Optical Communications — Theory and Practices. *Contemp. Issues*

Wirel. Commun. (2014). doi:10.5772/58884

46. Ambivalue. number and volume distributions in particle size analysis. (2017). Available at: https://www.ambivalue.com/site/assets/files/1017/eyetech-application-note-2017_02.pdf. (Accessed: 9th February 2021)

47. Alibolandi, M., Ramezani, M., Abnous, K., Sadeghi, F. & Hadizadeh, F. Comparative evaluation of polymersome versus micelle structures as vehicles for the controlled release of drugs. *J. Nanoparticle Res.* **17**, (2015).

48. Laan, A. C. & Denkova, A. G. Cryogenic transmission electron microscopy: the technique of choice for the characterization of polymeric nanocarriers. *EJNMMI Res.* **7**, 7–8 (2017).

49. Souza, T. G. F., Ciminelli, V. S. T. & Mohallem, N. D. S. A comparison of TEM and DLS methods to characterize size distribution of ceramic nanoparticles. *J. Phys. Conf. Ser.* **733**, (2016).

50. Liang, Y. *et al.* The effect of π-Conjugation on the self-assembly of micelles and controlled cargo release. *Artif. Cells, Nanomedicine Biotechnol.* **48**, 525–532 (2020).

51. Greenspan, P. & Fowler, S. D. Spectrofluorometric studies of the lipid probe, nile red. *J. Lipid Res.* **26**, 781–789 (1985).

52. Lampe, J. N., Fernandez, C., Nath, A. & Atkins, W. M. Nile red is a fluorescent allosteric substrate of cytochrome P450 3A4. *Biochemistry* **47**, 509–516 (2008).

53. Karukstis, K. K., Thompson, E. H. Z., Whiles, J. A. & Rosenfeld, R. J. Deciphering the fluorescence signature of daunomycin and doxorubicin. *Biophys. Chem.* **73**, 249–263 (1998).

54. Shah, S. *et al.* Fluorescence properties of doxorubicin in PBS buffer and PVA films. *PMC* 65–69 (2018). doi:10.1016/j.jphotobiol.2017.03.024.Fluorescence

55. Kaushik, D. & Bansal, G. Four new degradation products of doxorubicin: An application of forced degradation study and hyphenated chromatographic techniques. *J. Pharm. Anal.* **5**, 285–295 (2015).

56. Reinalda, L. *Design and Synthesis of Novel Oxidation Responsive Polymeric Micelles That Function as Nanocarriers for ROS- Mediated Drug Delivery*. (2019).

57. Tuo Wei, Chao Chen, Juan Liu, Cheng Liu, Paola Posocco, Xiaoxuan Liu, Qiang Cheng, Shuaidong Huo, Zicai Liang, Maurizio Fermeglia, View ORCID ProfileSabrina Pricl, Xing-Jie Liang, Palma Rocchi, and L. P. Supporting Information Anticancer drug nanomicelles formed by self-assembling amphiphilic dendrimer to combat cancer drug resistance. *PNAS* 1–5 (2015).

58. LTD, M. instruments. FAQ calculating volume distributions from DLS data. 1–4 Available at: https://www.materials-talks.com/wp-content/uploads/2017/01/FAQ-Calculating-volume-distributions-from-DLS-data.pdf. (Accessed: 9th February 2021)

59. Trimaille, T., Mondon, K., Gurny, R. & Möller, M. Novel polymeric micelles for hydrophobic drug delivery based on biodegradable poly(hexyl-substituted lactides). *Int. J. Pharm.* **319**, 147–154 (2006).

60. Hicks, M. & Gebicki, J. M. Rate constants for reaction of hydroxyl radicals with Tris, Tricine and Hepes buffers. *FEBS Lett.* **199**, 92–94 (1986).

Supplementary information

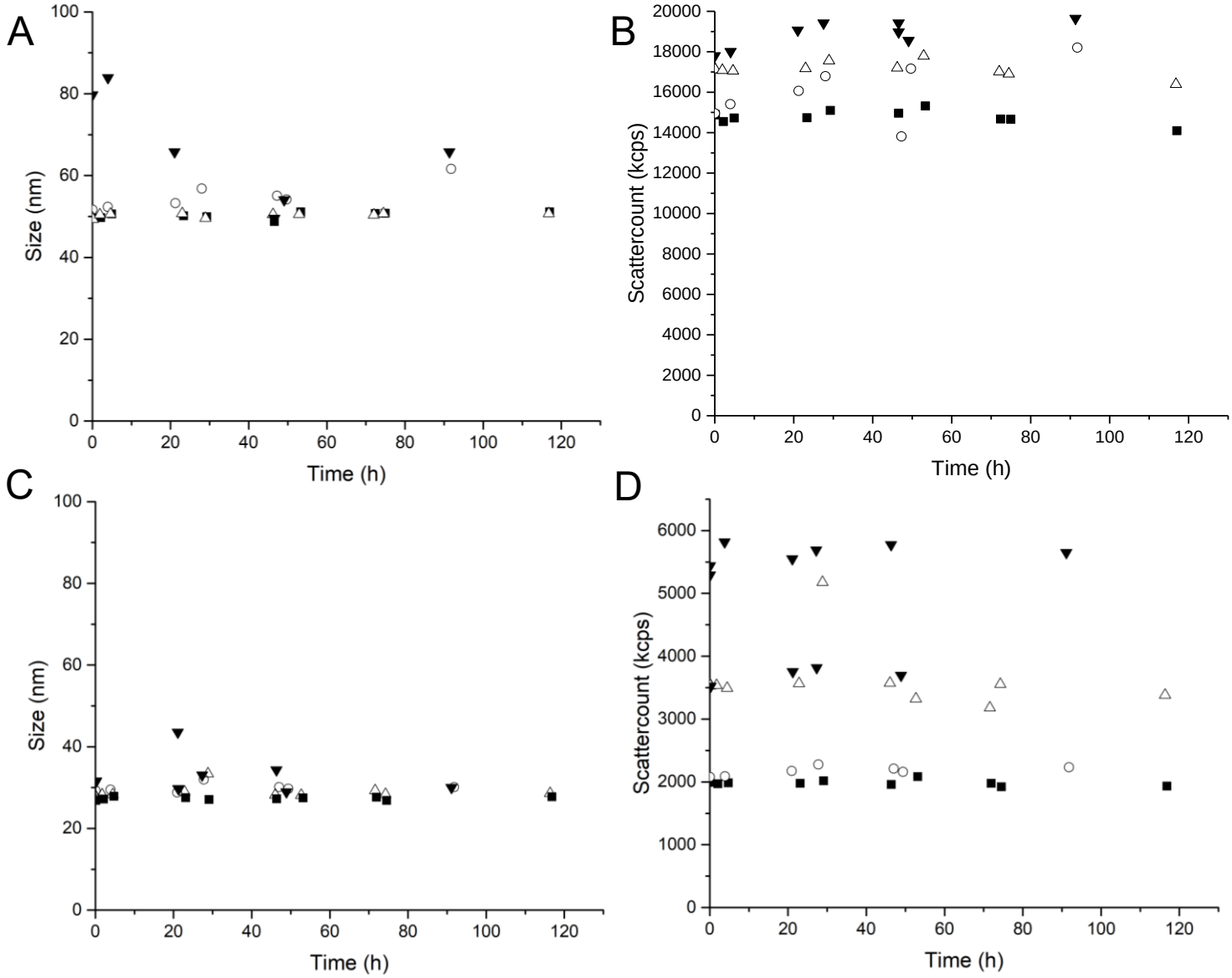

SI (4.1) (■=T=25°C; ○=T=37°C; △=T=25°C with NR; ▼=T=37°C with NR); A; Z-average of $PD_{85}M_{26}$ in PB, average size around 50nm, with elevated temperature and loaded NR the z-average increases slightly but stabilizes over time. B; Normalized scatter count of $PD_{85}M_{26}$ micelles, scattering count is consistent over time. C; Z-average of $PD_{130}M_{16}$ micelles, size is stable around 30 nm with elevated temperature and NR loading the z-average increases slightly but stabilizes over time. D; Normalized scattering count $PD_{130}M_{16}$ micelles, scattering count is not consistent for the R.T.

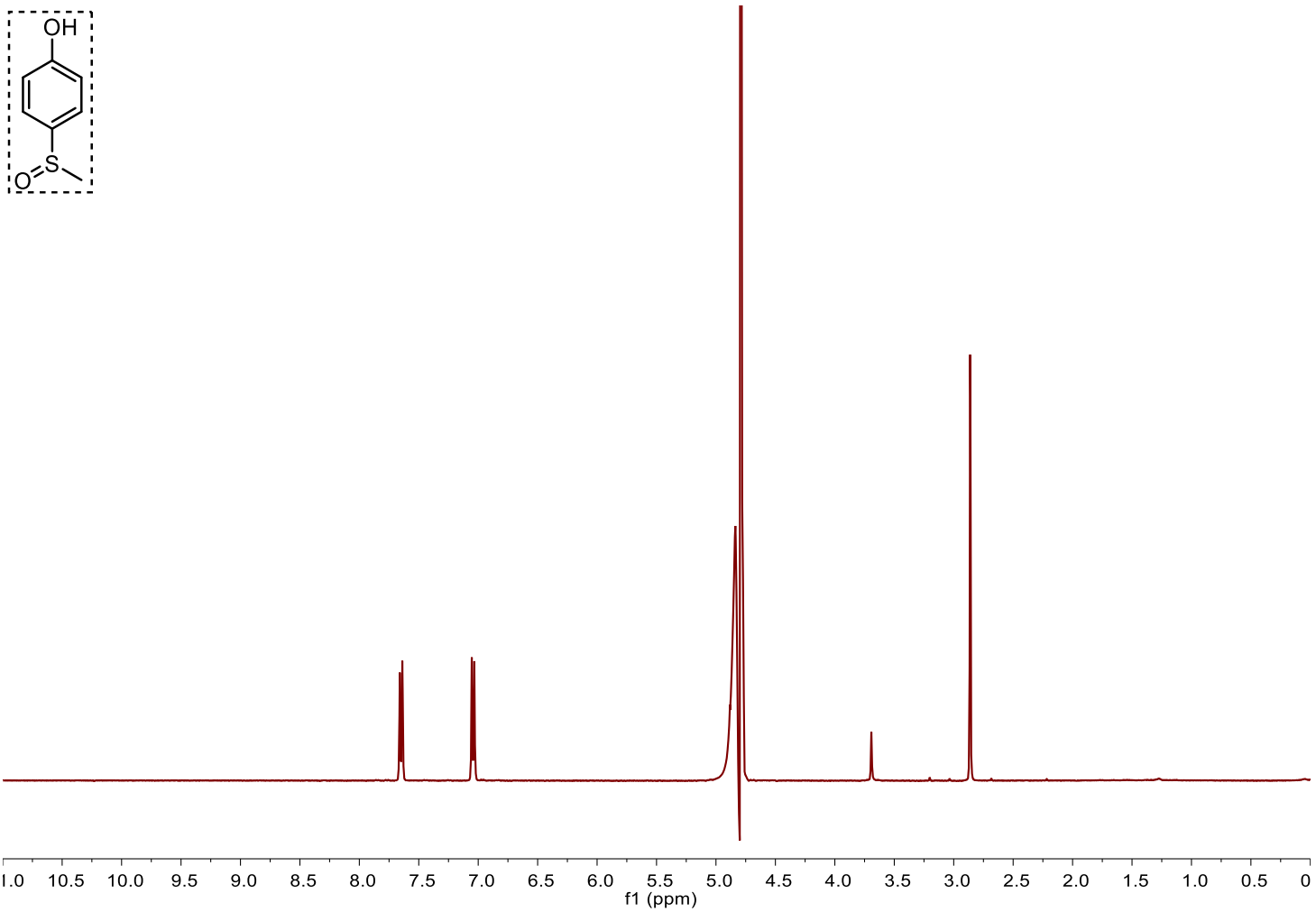

SI (4.2) (^{1}*H-NMR D_2O PB (1:9) mixture*) of 4-(methylsulfinyl)phenol (SOPh). [δ (ppm), D_2O] 7.66 (m,2H), 7.03 (m,2H), 2.86 (s,3H)]

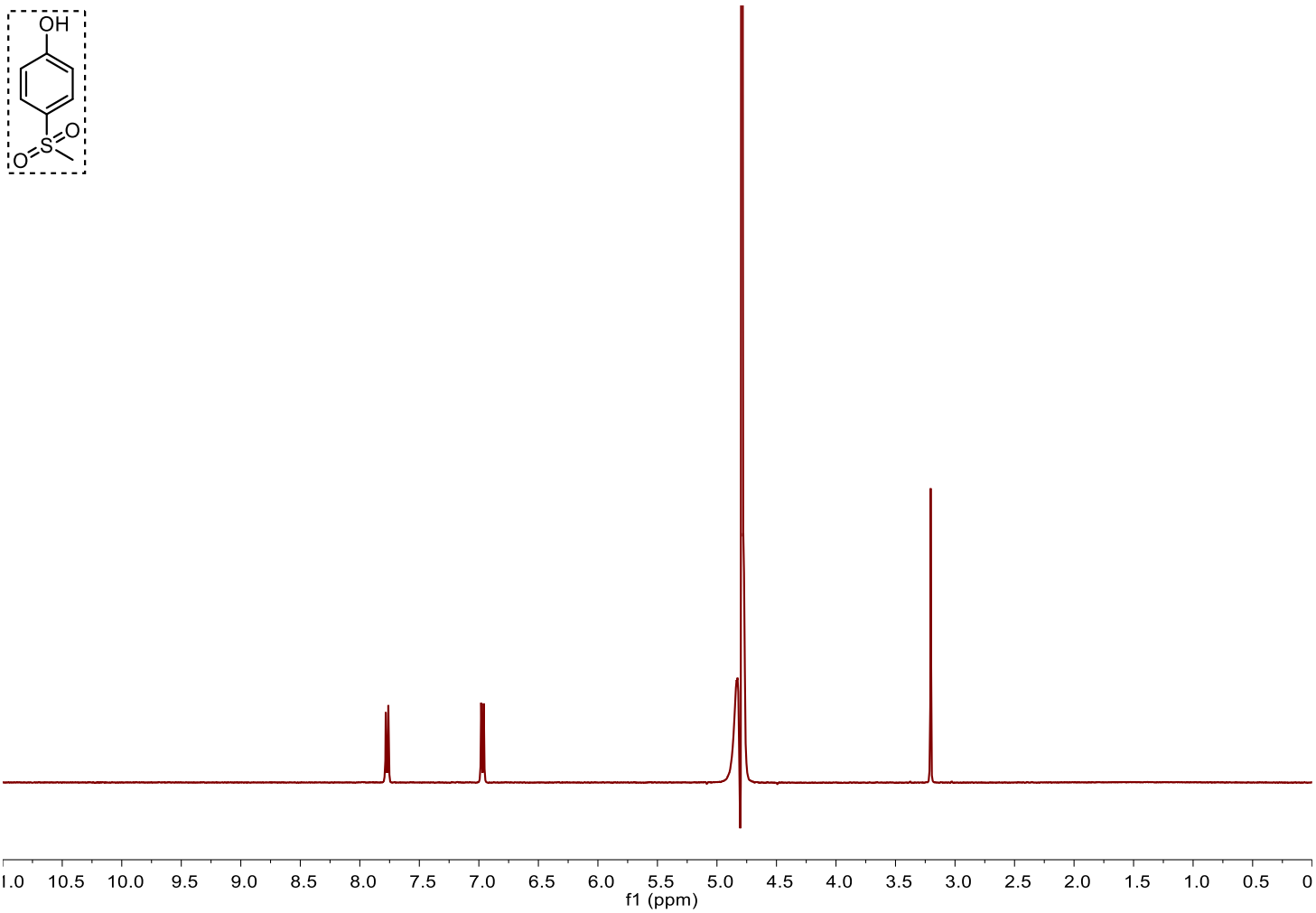

SI (4.3) (^{1}*H-NMR* D_2O*/PB (1:9) mixture*) of 4-(methylsulfonyl)phenol (SO2Ph). [δ (ppm), D_2O] 7.76 (m,2H), 6.98 (m,2H), 3.20 (s,3H)]

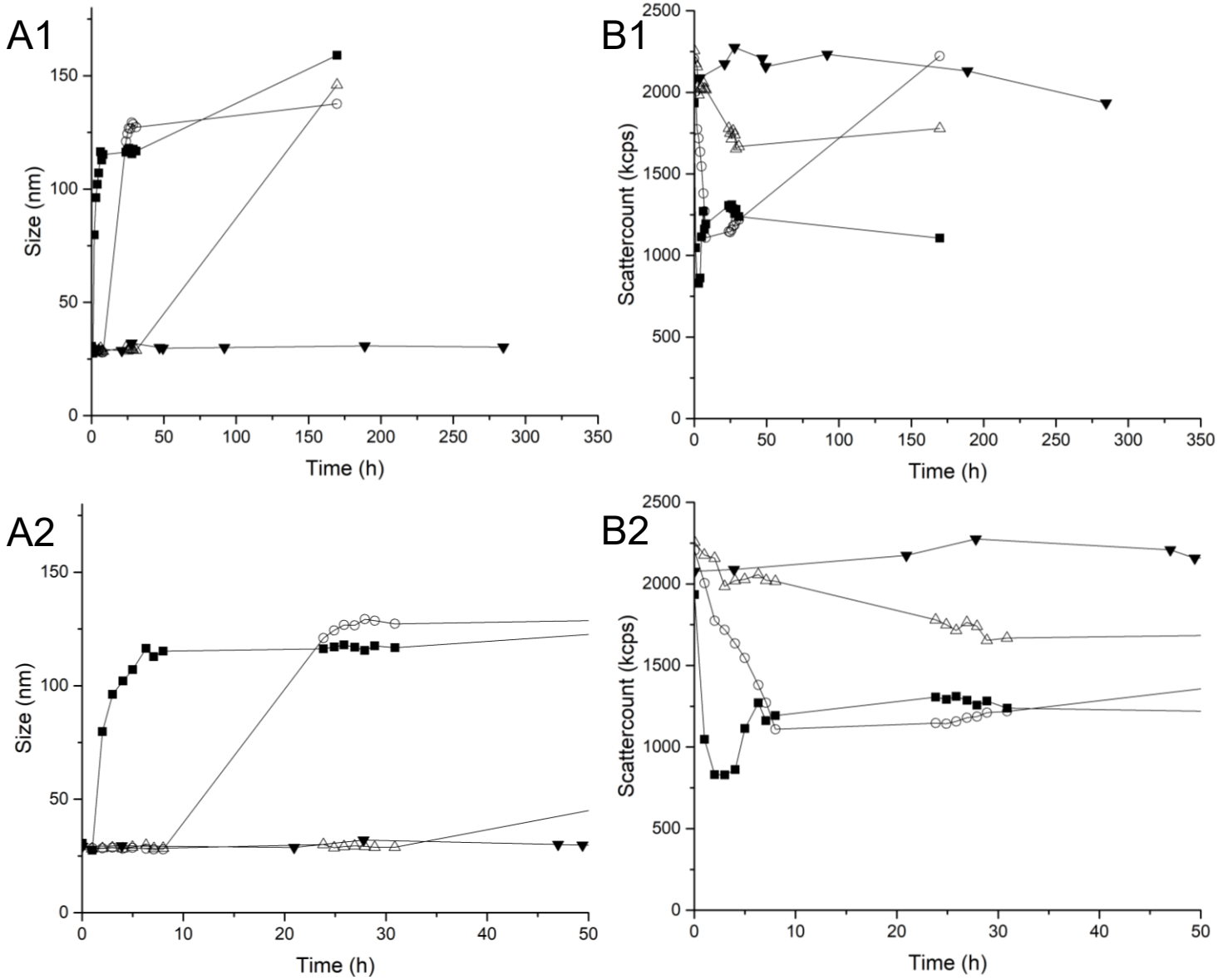

SI (4.4) Duplicate measurement of Fig (4.7) (■=2 wt% H_2O_2; ○= 0.2 wt% H_2O_2; △=0.007 wt% H_2O_2; ▼= Control) A1; Z-average after H_2O_2 addition for $PD_{130}M_{16}$, same trend is observed as in Fig 4.7. A2; Zoom on A1, same trend is observed as in fig 4.7. B1; Normalized scattering count for $PD_{85}M_{26}$ after H_2O_2 addition same trend is observed as in Fig 4.7 B2; Zoom on B1 same trend is observed as in fig 4.7.

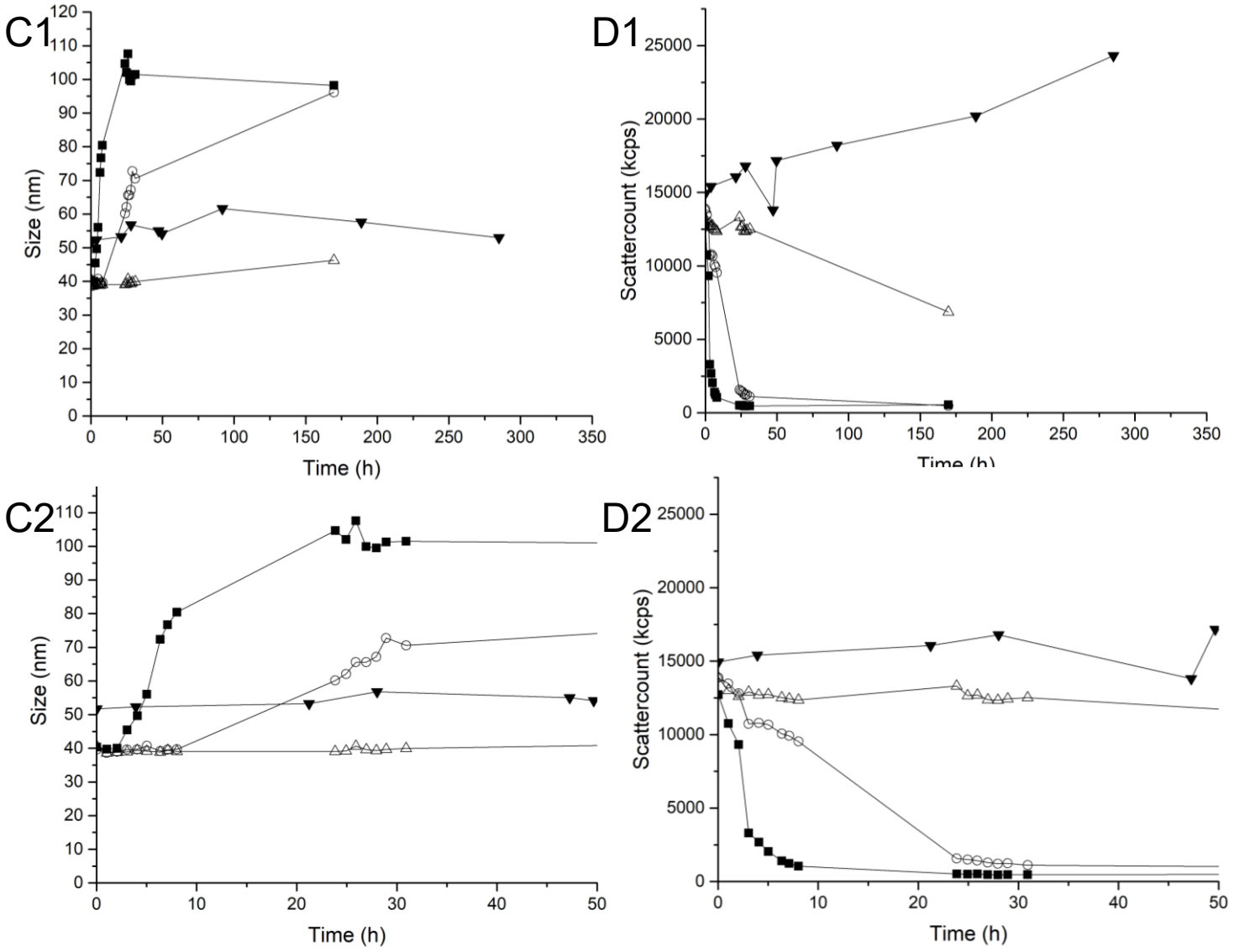

SI (4.5) Duplicate measurement of Fig (4.7) (■=2 wt% H_2O_2; ○= 0.2 wt% H_2O_2; △=0.007 wt% H_2O_2; ▼= Control) C1; Z-average after H_2O_2 addition for $PD_{85}M_{26}$, same trend is observed as in fig 4.7. C2; Zoom on C1 same trend is observed as in fig 4.7. D1; Normalized scattering count for $PD_{85}M_{26}$ after H_2O_2 addition, same trend is observed as in fig 4.7. D2; Zoom on D1 same trend is observed as in fig 4.7.

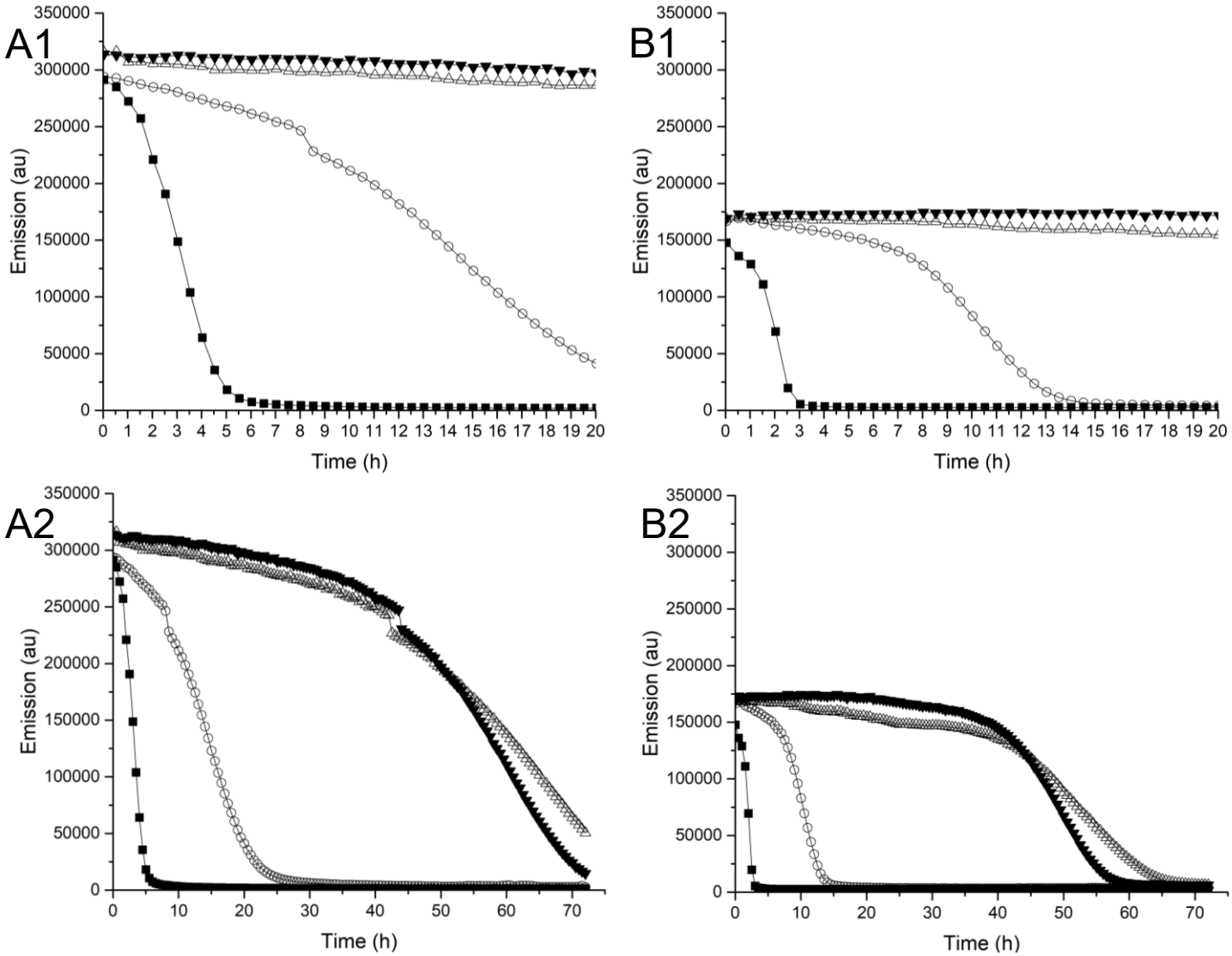

SI (4.6) (■=2 wt% H_2O_2; ○= 0.2 wt% H_2O_2; △=0.007 wt% H_2O_2; ▼= Control (0 wt% H_2O_2) Full measurement of Fig 4.10 NR emission at 633nm was traced over time A1; See fig 4.10 A2; full measurement of 72 hours, note drop around 250,000, probably caused by change in slit, after 24 hours a drop in NR emission in control and 0.007 wt% can be caused by drug leaking or NR degradation. B1; see Fig 4.10. B2; Full measurement of 72 hours, seems that 0.007 wt% initially causes NR release, but after 45 hours the control drops quicker than 0.007 wt%.

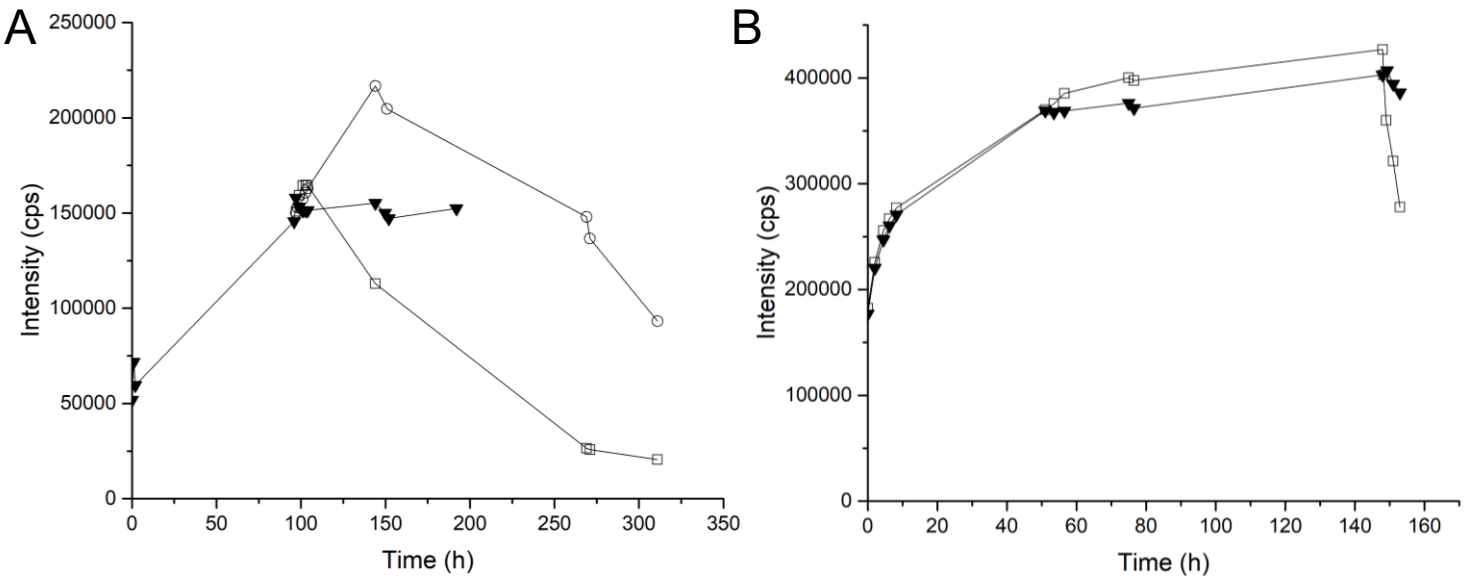

SI (4.7) Full measurement of Fig 4.12(▼= 0 wt% H_2O_2, □ = 2 wt% H_2O_2, ○=0.2 wt% H_2O_2) A; $PD_{130}M_{16}$ with DOX at R.T. after 96 hours of initial passive release H_2O_2 was added. B; DOX without $PD_{130}M_{16}$ at R.T. after 148 hours of initial passive decomposition of probably DOX aggregates, H_2O_2 was added.

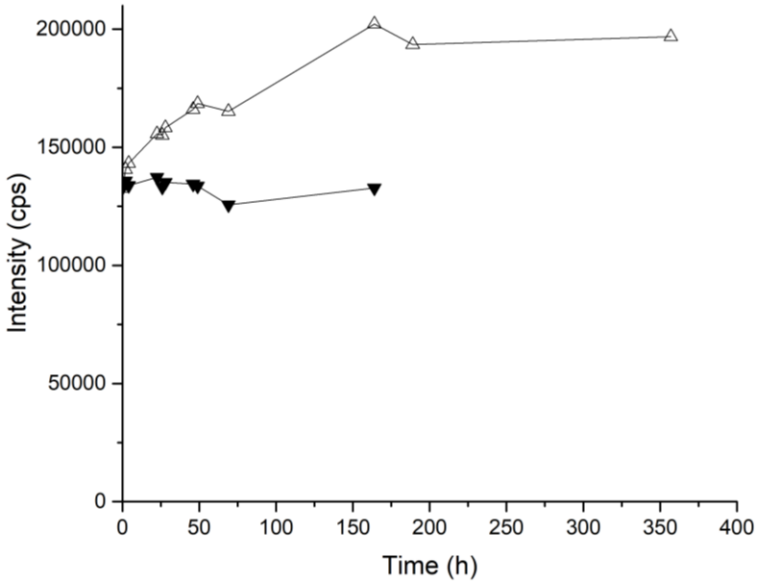

SI (4.8) continuation of Fig 4.12 Emission of DOXs maximum at 590nm over time (▼= 0 wt% H_2O_2, △= 0.007 wt% H_2O_2) $PD_{130}M_{16}$ with DOX at R.T. >140 hours after dilution, H_2O_2 was added (at Time=0h). Direct increase of fluorescence is observed which does not decrease as much as 0.2 wt% and 2 wt% H_2O_2 addition.

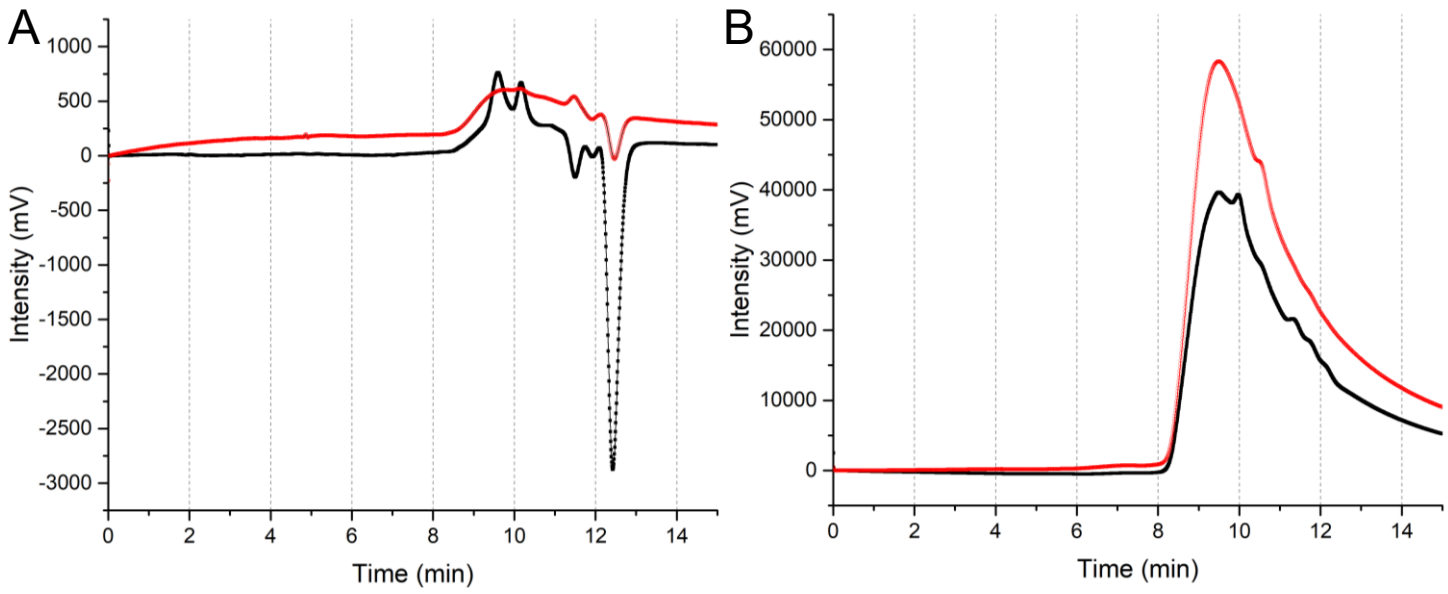

SI (4.8) GPC with THF A; Refractive index intensity expressed in mV. $PD_{130}M_{16}$ (red) dissolved in THF, was compared by $PD_{130}M_{16}$ with 500 Gy ^{60}Co radiation dissolved in THF (black). Broad peak arising between 8 and 9 min became after radiation sharper and divided in 2 little peaks, indicating that 500 Gy did influence the polymer directly. B; Absorbance at 255nm, $PD_{130}M_{16}$ (red) dissolved in THF, was compared by $PD_{130}M_{16}$ with 500 Gy ^{60}Co radiation dissolved in THF (black). A lot of absorbance was detected probably due to the MTPA region of the polymer, the big broad peak became 2 peaks after radiation, concluding that radiation did influence the polymer.

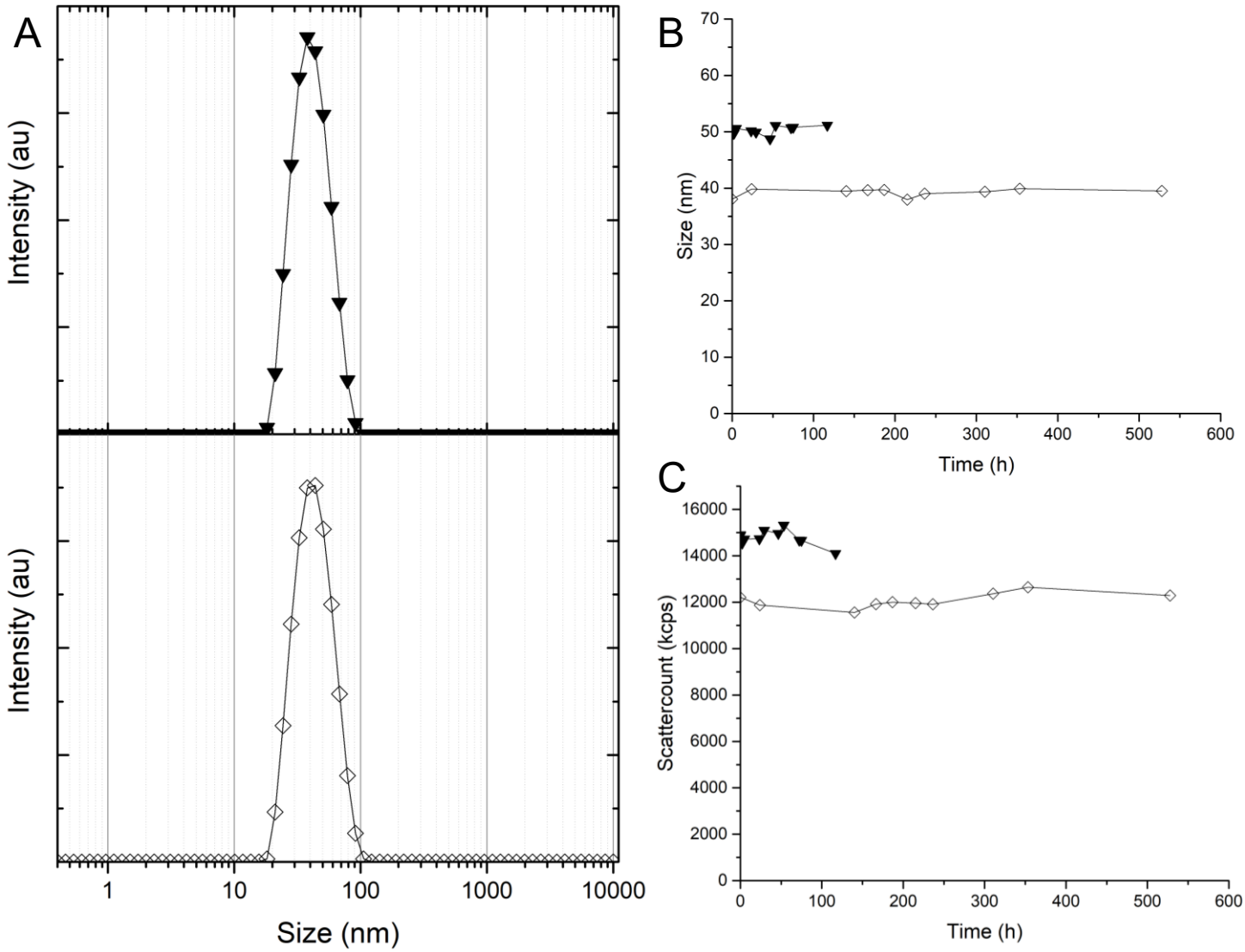

SI (4.9) $PD_{85}M_{26}$ in PB (▼= control, ◇= 67 Gr) A; Light intensity plot with 0 Gy and 67 Gr, no change is observed indicating that external radiation does not influence the size for $PD_{85}M_{26}$ micelles. B; Z-average difference between 0 Gy and 67 Gy is due to the difference in batch, both stable and unchanged over time. C; Scatter count for 0Gy and 67 Gy stable no change observed over time. Difference due to different batch of 0 Gy and 67 Gy.

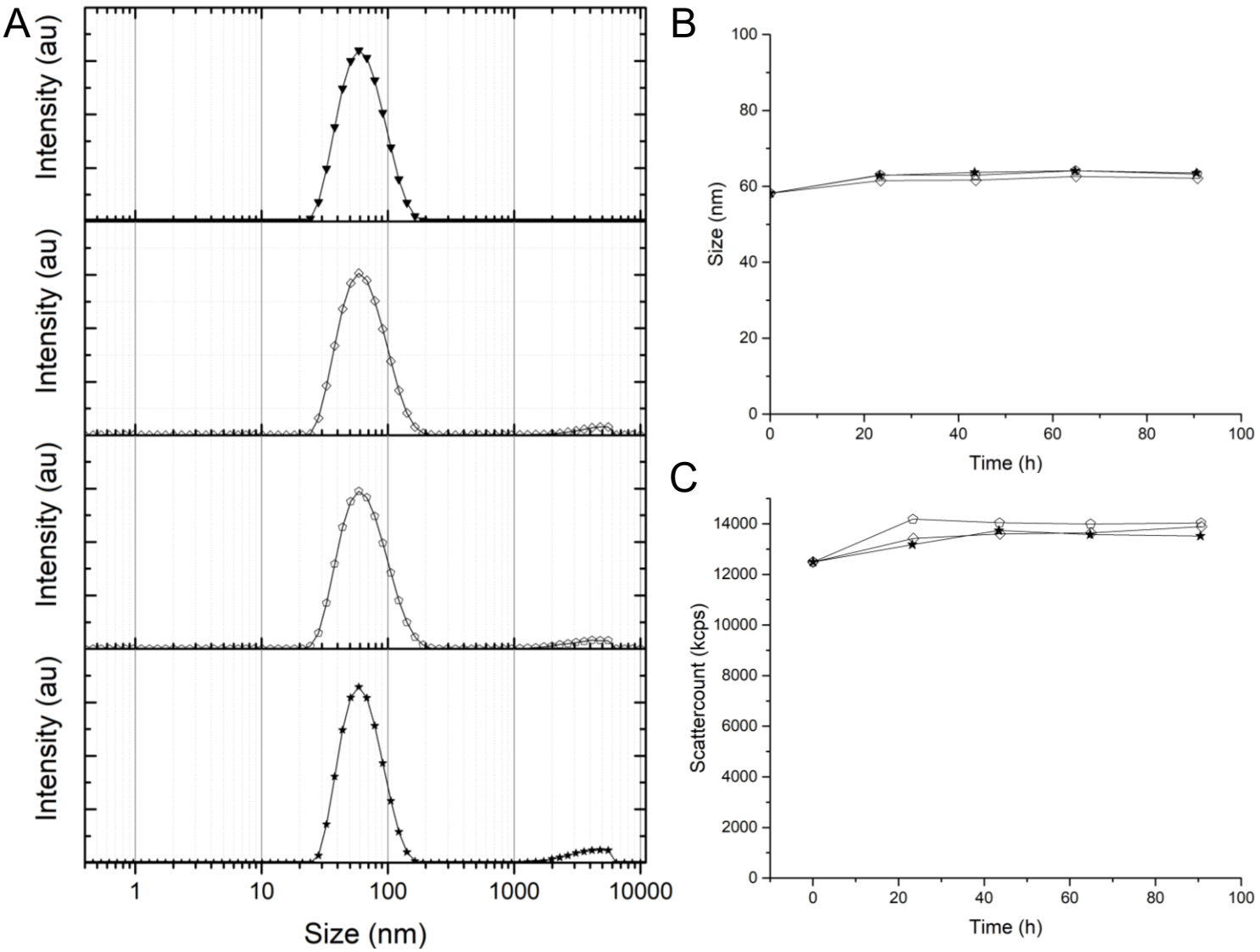

SI (4.10) (▼= Control, ◇= 82 Gr, ⬡= 120 Gr, ★=500Gr) $PD_{85}M_{26}$ in HEPES. A; Light intensity plot with 0Gy up to 500 Gy in HEPES. With radiation a small peak arises between 2000 and 6000 nm but, almost insignificant compared with the dominant micelles peak. B; Z- average over time is stable, no control was made over time. Size is different compared to previous measurement, maybe caused by different solvent (PB vs HEPES). C; Scattering count slightly increased after radiation caused by formation of few bigger particles but insignificant.

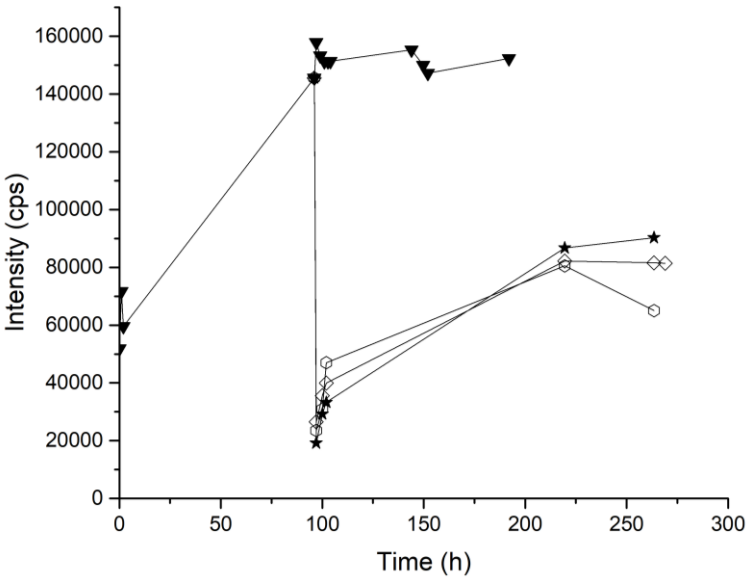

SI (4.11) Full spectrum of Fig (4.16) (▼=0 Gr, ◇= 60Gr, ⬡= 120 Gr, ★= 500 Gr) Emission maximum DOX in $PD_{130}M_{16}$ in PB at R.T., after initial 96 hours of passive decomposition of DOX aggregates samples got radiated by ^{60}Co source. See fig 4.16.

H_2O_2 wt%	mol/kg	M	mM
2.0	0.59	0.59	593.82
0.20	0.06	0.06	58.65
0.020	0.01	0.01	5.86
0.0070	0.00	0.00	2.05

SI (4.12) Conversion of H_2O_2 weight percentage to concentration in mM, densities of 0.007 wt% up to 0.2 wt% H_2O_2 are considered equal to have a density equal to 100% H_2O (0.997 g/ml), Density of 2 wt% H_2O_2 is 1.0095 gr/ml.